Med

CellPress

Clinical and Translational Article

Discovery and intranasal administration of a SARS-CoV-2 broadly acting neutralizing antibody with activity against multiple Omicron subvariants

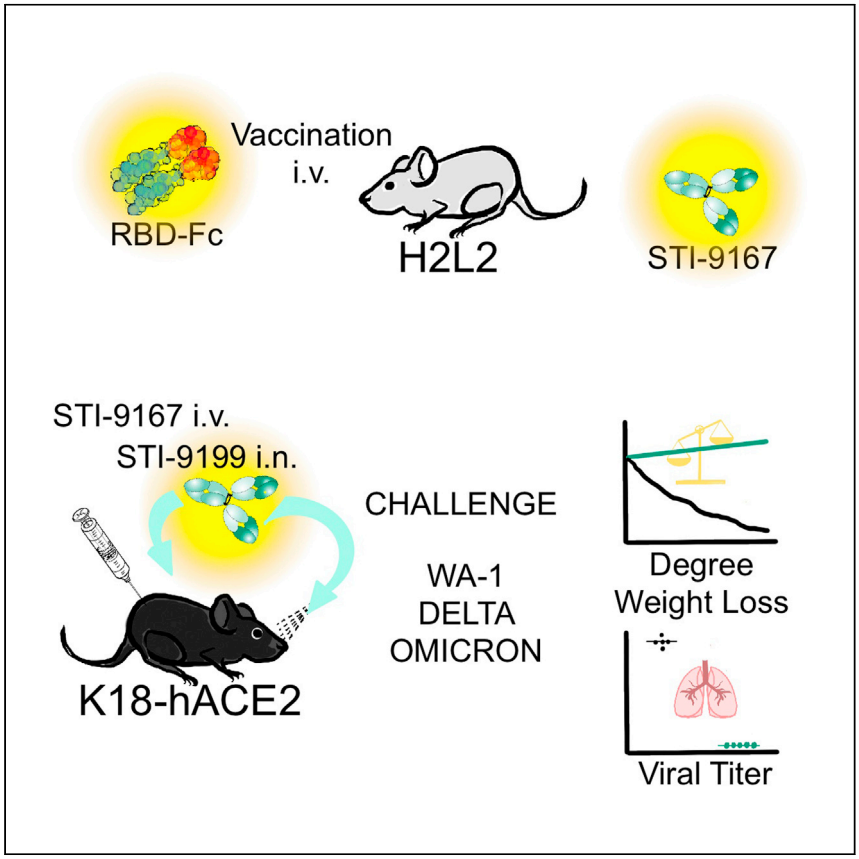

The burden of COVID-19 and the emergence of virus variants necessitates continued exploration of neutralizing antibody therapies and methods of treatment. Duty et al. identify a human monoclonal antibody that neutralizes recently described SARS-CoV-2 variants and, when administered intranasally or intravenously, offers protection in a mouse model of SARS-CoV-2 disease.

Pre-clinical Research

J. Andrew Duty, Thomas Kraus, Heyue Zhou, ..., Henry Ji, Domenico Tortorella, Robert Allen

hji@sorrentotherapeutics.com

Highlights

A neutralizing antibody retains activity across BA.1 and BA.2 subvariants

Therapeutic protection against WA-1, Delta, and Omicron pathogenesis in K18-hACE2 mice

Equivalent efficacy of i.n.- and i.v.-delivered SARS-CoV-2 neutralizing antibody therapy

Duty et al., Med 3, 705–721
October 14, 2022
https://doi.org/10.1016/j.medj.2022.08.002

Med

CellPress

Clinical and Translational Article

Discovery and intranasal administration of a SARS-CoV-2 broadly acting neutralizing antibody with activity against multiple Omicron subvariants

J. Andrew Duty,[2,3,12] Thomas Kraus,[2,3,12] Heyue Zhou,[1,12] Yanliang Zhang,[1,12] Namir Shaabani,[1,12] Soner Yildiz,[2,5] Na Du,[1] Alok Singh,[1] Lisa Miorin,[2,5] Donghui Li,[1] Karen Stegman,[1] Sabrina Ophir,[2] Xia Cao,[1] Kristina Atanasoff,[2,6] Reyna Lim,[1] Ignacio Mena,[2] Nicole M. Bouvier,[2,11] Shreyas Kowdle,[2] Juan Manuel Carreño,[2] Laura Rivero-Nava,[1] Ariel Raskin,[2] Elena Moreno,[2] Sachi Johnson,[1] Raveen Rathnasinghe,[2,6] Chin I. Pai,[1] Thomas Kehrer,[2,6] Elizabeth Paz Cabral,[1] Sonia Jangra,[2] Laura Healy,[1] Gagandeep Singh,[2] Prajakta Warang,[2] Viviana Simon,[2,5,7,8] Emilia Mia Sordillo,[8] Harm van Bakel,[10] Yonghong Liu,[2] Weina Sun,[2] Lisa Kerwin,[1] John Teijaro,[4] Michael Schotsaert,[2,5] Florian Krammer,[2,8] Damien Bresson,[1] Adolfo García-Sastre,[2,5,7,8,9] Yanwen Fu,[1] Benhur Lee,[2] Colin Powers,[1] Thomas Moran,[2,3] Henry Ji,[1,13,*] Domenico Tortorella,[2,3] and Robert Allen[1]

SUMMARY

Background: The continual emergence of severe acute respiratory syndrome coronavirus 2 (SARS-CoV-2) variants of concern, in particular the newly emerged Omicron (B.1.1.529) variant and its BA.X lineages, has rendered ineffective a number of previously FDA emergency use authorized SARS-CoV-2 neutralizing antibody therapies. Furthermore, those approved antibodies with neutralizing activity against Omicron BA.1 are reportedly ineffective against the subset of Omicron subvariants that contain a R346K substitution, BA.1.1, and the more recently emergent BA.2, demonstrating the continued need for discovery and characterization of candidate therapeutic antibodies with the breadth and potency of neutralizing activity required to treat newly diagnosed COVID-19 linked to recently emerged variants of concern.

Methods: Following a campaign of antibody discovery based on the vaccination of Harbor H2L2 mice with defined SARS-CoV-2 spike domains, we have characterized the activity of a large collection of spike-binding antibodies and identified a lead neutralizing human IgG1 LALA antibody, STI-9167.

Findings: STI-9167 has potent, broad-spectrum neutralizing activity against the current SARS-COV-2 variants of concern and retained activity against each of the tested Omicron subvariants in both pseudotype and live virus neutralization assays. Furthermore, STI-9167 nAb administered intranasally or intravenously provided protection against weight loss and reduced virus lung titers to levels below the limit of quantitation in Omicron-infected K18-hACE2 transgenic mice.

Conclusions: With this established activity profile, a cGMP cell line has been developed and used to produce cGMP drug product intended for intravenous or intranasal use in human clinical trials.

Funding: Funded by CRIPT (no. 75N93021R00014), DARPA (HR0011-19-2-0020), and NCI Seronet (U54CA260560).

CONTEXT AND SIGNIFICANCE

COVID-19 infection remains an ongoing concern for the global population, where development of new treatments remains critical as new variants emerge. Using *in vitro* systems and a mouse model of COVID-19 infection, researchers at Sorrento Therapeutics and Mount Sinai identified novel neutralizing antibodies that potently neutralized different variants of COVID-19 including Omicron subvariants BA.1, BA.1.1, and BA.2. Importantly, the neutralizing antibody was protective when administered either intravenously or intranasally in the mouse model of COVID-19 infection. This suggests that future COVID-19 antibody therapies could effectively utilize an intranasal route of therapeutic delivery and retain efficacy.

INTRODUCTION

The severe acute respiratory disease syndrome coronavirus 2 (SARS-CoV-2) pandemic has continued to significantly impact the health and lives of people around the globe.[1] To date, public health agencies have sought to combat infections leading to coronavirus disease 2019 (COVID-19) by relying on quarantine, social distancing, vaccination, and antiviral countermeasure strategies.[2,3] Despite these efforts, the continued spread of SARS-CoV-2 has led to the emergence of several variants of concern (VOC) that have risen in prevalence worldwide.[2–7]

Most VOC encode multiple changes in the amino acid sequence of the SARS-CoV-2 spike that can impact the neutralizing properties of manufactured SARS-CoV-2 neutralizing antibodies (nAbs) as well as nAbs elicited following vaccination or during the course of natural infection. Specifically, the Omicron VOC (B.1.1.529 BA.1) live virus, when profiled *in vitro* using Vero cells expressing human angiotensin converting enzyme 2 (ACE2) and human transmembrane serine protease 2 (TMPRSS2) for susceptibility to nAbs currently authorized or approved for clinical use (AFCU nAbs), are resistant to the neutralizing activities of REGN10987 (imdevimab), REGN10933 (casirivimab), LY-CoV555 (bamlanivimab), LY-CoV016 (etesevimab), and CT-P59 (regdanvimab) at nAb concentrations $\leq$10 μg/mL (half-maximal inhibitory concentration [IC_{50}]) and remained susceptible to nAbs COV2-2130 (cilgavimab) and COV2-2196 (tixagevimab) tested as single nAb therapies or in combination (IC_{50} = 43, 126, and 181 ng/mL, respectively).[8–13] In live virus neutralization assays utilizing Vero cells overexpressing human TMPRSS2, S309 (sotrovimab) registered an IC_{50} of 373 ng/mL, consistent with previously published activity in Omicron pseudovirus particle entry inhibition assays.

Omicron lineage viruses that encode an additional signature mutation in the SARS-CoV-2 spike at position R346K in the receptor binding domain (RBD) of the protein, termed B.1.1.529 BA.1.1 (BA.1.1), represented nearly 40% of Omicron sequences reported to GISAID by mid-February, 2022.[14–17] The R346K mutation was previously identified among the defining mutations of the SARS-CoV-2 Mu (B.1.621) VOC.[7] More recently, the Omicron subvariant, B.1.1.529 BA.1.2 (BA.2), and subvariants thereof have continually increased in prevalence among newly reported infections (GISAID). Using BA.1.1 pseudotyped virus particles, neutralization potency was reported as substantially reduced for all tested AFCU nAbs, including COV2-2130, COV2-2196, and S309.[5,18–21] Current antibodies in development, including LY-CoV1404 (bebtelovimab) and BRII-198 (romlusevimab), maintain activity in Omicron BA.1 pseudotyped particle neutralization assays.[12,22] BRII-198 displays substantially reduced neutralizing activity in assays using BA.1.1 and BA.2 pseudoviruses, while testing of LY-CoV1404 against the BA.1.1 and BA.2 subvariants has shown this antibody to maintain activity against each of these subvariants.[12,17,22] As such, there is a continued need for discovery and development of nAbs that can provide potent immune protection against COVID-19 caused by pandemic VOC presently infecting the global population.

In the early COVID-19 clinical setting, intravenous (i.v.) administration of nAbs was an effective means of lessening progression and overall severity of disease.[19,23] As COVID-19 is a predominantly respiratory disease, exploration of alternative modes of antibody administration, including intranasal (i.n.) delivery, may provide an expedient means of delivering antibodies and increasing the respiratory tract bioavailability of anti-COVID-19 nAbs, as well as augmenting the developing host-directed immune response to prevent exacerbation of clinical symptoms and hospitalization.[24–26]

[1]Sorrento Therapeutics, Inc., San Diego, CA 92121, USA

[2]Department of Microbiology, Icahn School of Medicine, Mount Sinai, New York, NY, USA

[3]Center for Therapeutic Antibody Development, Drug Discovery Institute, Icahn School of Medicine, Mount Sinai, New York, NY, USA

[4]Department of Immunology and Microbial Science, The Scripps Research Institute, La Jolla, CA 92037, USA

[5]Global Health and Emerging Pathogens Institute, Icahn School of Medicine, Mount Sinai, New York, NY, USA

[6]Graduate School of Biomedical Sciences, Icahn School of Medicine at Mount Sinai, New York, NY, USA

[7]Department of Medicine, Division of Infectious Diseases, Icahn School of Medicine at Mount Sinai, New York, NY, USA

[8]Department of Pathology, Molecular and Cell-Based Medicine, Icahn School of Medicine at Mount Sinai, New York, NY, USA

[9]The Tisch Cancer Institute, Icahn School of Medicine, Mount Sinai, New York, NY, USA

[10]Department of Genetics and Genomic Sciences, Icahn School of Medicine, Mount Sinai, New York, NY, USA

[11]Division of Infectious Diseases, Department of Medicine, Icahn School of Medicine, Mount Sinai, New York, NY, USA

[12]These authors contributed equally

[13]Lead contact

*Correspondence: hji@sorrentotherapeutics.com

https://doi.org/10.1016/j.medj.2022.08.002

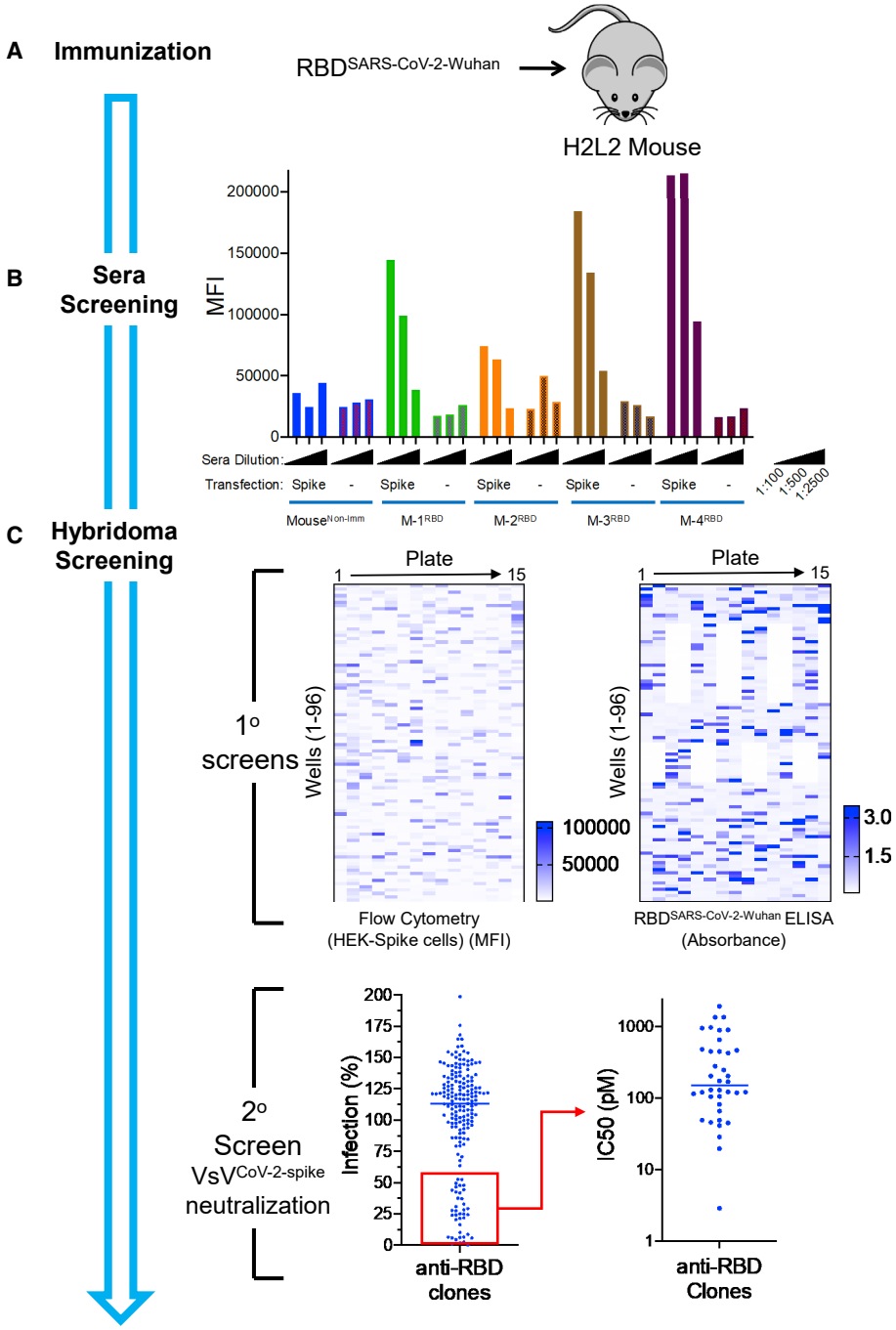

Human anti-SARS CoV-2 antibody families				
Family	Clone (#s)	VsV-CoV2-spike (IC50)	VDJ (Heavy)	VJ (Kappa)
A	2	490-1000pM	VH3-53/DH6-19/JH3	VK1-9/JK2
B	16	50-440pM	VH1-8/DH3-10/JH6	VK3-20/JK5
D	1	1pM	VH3-49/DH6-13/JH4	VK3-15/JK1
E	4	70-125pM	VH4-4/DH3-19/JH4	VK3-15/JK2
F	1	115pM	VH3-53/DH3-9/JH6	VK3-15/JK4
G	6	5-130pM	VH3-33/DH2-21/JH4	VK1-39/JK1

Figure 1. Rapid discovery of neutralizing antibodies

(A and B) (A) Harbor H2L2 Mice (M-1, -2, -3, -4) were immunized and boosted 2× with SARS-CoV-2 RBD (Wuhan-1 strain) and (B) sera (1:100, 1:500, and 1:2,500) from these mice were analyzed by flow cytometry from Expi293F untransfected or transfected with the SARS-CoV-2 spike. As a control, serum from a non-immunized mouse was used.

(C) Primary screens based on the anti-RBD clones from mouse 4 (M-4) were performed using flow cytometry using HEK293 cells transfected with spike protein and RBD ELISA. Upon flow cytometry analysis, the MFI was determined for each clone. The RBD ELISA represents binding of the clones to RBD as measured by absorbance. Both the flow cytometry and ELISA data are represented as heatmaps. The secondary assays for the binding clones were a neutralization assay using VSV-spike^{CoV-2} followed by a determination of IC_{50} (pM) for clones with >50% neutralization activity.

(D) The clones with IC_{50} values <500 pM were sequenced and mAb clones were identified by specific V(D)J gene-segment combinations and junction (CDR3) characteristics, which allowed them to be grouped into different clonal families (family "A-B &D-G").

Data presented herein demonstrate the identification, *in vitro* binding, and potent neutralizing activity of STI-9167 against live viruses and pseudotype viruses representing the current catalog of SARS-CoV-2 variants, including the Omicron BA.1, BA.1.1, and BA.2 subvariants. In addition, we describe the protective effects of STI-9167 administered i.v. or i.n. in the K18ACE2 transgenic mouse model of COVID-19 disease following challenge with either the WA-1 strain, Delta or (B.1.617.2), or the Omicron BA.1 VOC.

RESULTS

Generation of human anti-SARS-CoV-2 spike antibodies

To generate a panel of neutralizing human monoclonal antibodies against SARS-CoV-2, Harbor *H2L2* mice were immunized and boosted with an RBD fusion protein based on the original spike glycoprotein sequence from the Wuhan-1 spike glycoprotein sequence (GenBank accession no. MN908947), which was fused to a mouse Fc domain (Figure 1A). The sera from immunized mice were assessed for binding to 293ExpiF cells transfected with SARS-CoV-2 spike cDNA (Wuhan-1) using high-throughput flow cytometry (Figure 1B). We observed that the serum from mice 1, 3, and 4 demonstrated a concentration-dependent and specific binding to 293ExpiF cells expressing the SARS-CoV-2 spike. Given that mouse 3 and mouse 4 had the highest antibody titer response against the SARS-CoV-2 spike, the spleens from these animals were used to generate hybridoma clones.[27] The hybridoma clones (1,824 clones from mouse 3 and 1,440 clones from mouse 4) were screened for binding to 293ExpiF cells expressing SARS-CoV-2 spike by flow cytometry and RBD spike (Wuhan-1) by ELISA (Figures 1C and S1). A representative heatmap for mouse 4 fusion was generated to summarize the mean fluorescence intensity (MFI) for each hybridoma clone (Figure 1C). In parallel, hybridoma clones were subjected to an RBD enzyme-linked immunosorbent assays (ELISA) validating the clones that bound to the SARS-CoV-2 spike. We identified 188 clones with a >5-fold MFI over untransfected cells and classified these as candidate SARS-CoV-2 binding antibodies.

The supernatants from these clones were then evaluated in a high-throughput neutralization assay using the replication competent vesicular stomatitis virus (VsV) reporter virus that utilizes SARS-CoV-2 spike (VsV$^{CoV2-spike}$) as its envelope protein and expressing GFP as readout for infection[28] (Figure 1C, secondary screening). In brief, VsV$^{CoV2-spike}$ was pre-incubated with hybridoma supernatant (1:20) followed by infection of HEK293 cells expressing ACE2 and TMPRSS2 for 24 h and analyzed for GFP-positive cells using flow cytometry. The percent infection was determined by assigning 100% infection with VsV$^{CoV2-spike}$ pre-incubated with hybridoma medium alone. Thirty-eight clones that decreased infection by >50% were selected for further evaluation for neutralization by determining the IC_{50} values. For the hybridomas from the mouse 3 fusion, 340 clones were found to bind to the SARS-CoV-2 spike and 90 clones were found to have neutralization activity against VsV$^{CoV2-spike}$ (Figure S1). The selected neutralizing clones with IC_{50} values < 125

pM were then examined for IgG isotypes and expanded for further analysis. Sequencing of the IgG heavy chain from each hybridoma clone revealed diverse CDR3 lengths (10–20 aa in length) and variable genes (Figure 1D). Clones that were identical copies of each other were consolidated to a single candidate.

To identify the most effective human anti-SARS-CoV-2 spike nAbs, we performed a $VsV^{CoV2-spike}$ neutralization assay (Figure 1D). $VsV^{CoV2-spike}$ pre-incubated with increasing concentrations of antibody (0–2.5 μg/mL) was added to human ACE2/TMPRSS2-expressing HEK293 cells and analyzed for GFP-positive cells using flow cytometry.

$VsV^{CoV2-spike}$ pre-incubated with a control antibody was used as 100% infection. The various unique antibodies have a range of IC_{50} values from 5 to 1,000 pM across the different antibody families (Figures 1D and S2). Collectively, we have identified a panel of unique human antibodies that bind to SARS-CoV-2 and effectively neutralize a reporter virus that utilizes the SARS-CoV-2 spike for entry into human cells.

Candidate nAb sequences were formatted from the human/rat chimera isolated from the Harbor animals as full-length human IgG1 antibodies and expressed in Chinese hamster ovary cells for further characterization *in vitro*. In fact, virus-specific antibodies can lead to exacerbation of disease symptoms through a process termed antibody-dependent enhancement (ADE).[29,30] To reduce the risk of ADE resulting from administration of our lead candidate STI-9167, the IgG1 Fc regions were modified by introducing specific amino acid substitutions (L234A, L235A [LALA]).[31,32] The LALA Fc modification reduces binding affinity to Fcγ receptors while providing a similar blockade to interactions between SARS-CoV-2 and the ACE2 receptor expressed on susceptible cells in the lung and other organs.[33–35]

To determine the effects of variant-specific spike S1 domain mutations within and outside the RBD region of S1 on antibody binding, the affinity of STI-9167 and antibodies synthesized based on available sequences of EUA-approved SARS-CoV-2 reference clone nAbs S309 (sotrovimab), COV2-2130 (cilgavimab), COV2-2196 (tixagevimab), and LY-CoV1404 was determined for monomeric WA-1 spike S1 subunit binding as well as VOC-derived S1 domains using surface plasmon resonance (SPR) (Figures 2A, S3A, and S3B; Table 1). Of note, the k_D of STI-9167 was measured as 6.20 nM for the WA-1 isolate, 4.45 nM for the Delta variant, and 22.6 nM for the Omicron BA.1 subvariant. Binding kinetics for the Omicron variant were compared between STI-9167, S309, COV2-2130, and COV2-2196 (Figures 2A and S3A; Table 1). STI-9167 and COV2-2130 had a similar association rate and the rate for S309 was approximately 5-fold slower. The dissociation rate was slowest with S309 by a factor of approximately 10-fold compared with STI-9167, and STI-9167 dissociated at an approximately 2-fold slower rate than COV2-2130. COV2-2196 binding to Omicron BA.1 S1 domain monomer was insufficient to allow for quantitation.

In an effort to assess nAb binding to spike proteins in a native conformation, STI-9167 was tested for the binding of full-length spike protein expressed on the surface of transfected HEK293 cells. Cell-based binding studies demonstrated that STI-9167 binds with similar efficiency to the surface-expressed spike from the WA-1 isolate (half-maximal effective concentration, EC_{50} = 0.025 μg/mL), the Delta variant (EC_{50} = 0.011 μg/mL), the Omicron BA.1 subvariant (EC_{50} = 0.025 μg/mL), the BA.1.1 subvariant (EC_{50} = 0.024 μg/mL), and the BA.2 subvariant (EC_{50} = 0.04 μg/mL), as well as the greater catalog of VOC spike protein (Figures 2B and S3C). In general, the rank-order of binding efficiencies to the surface-expressed

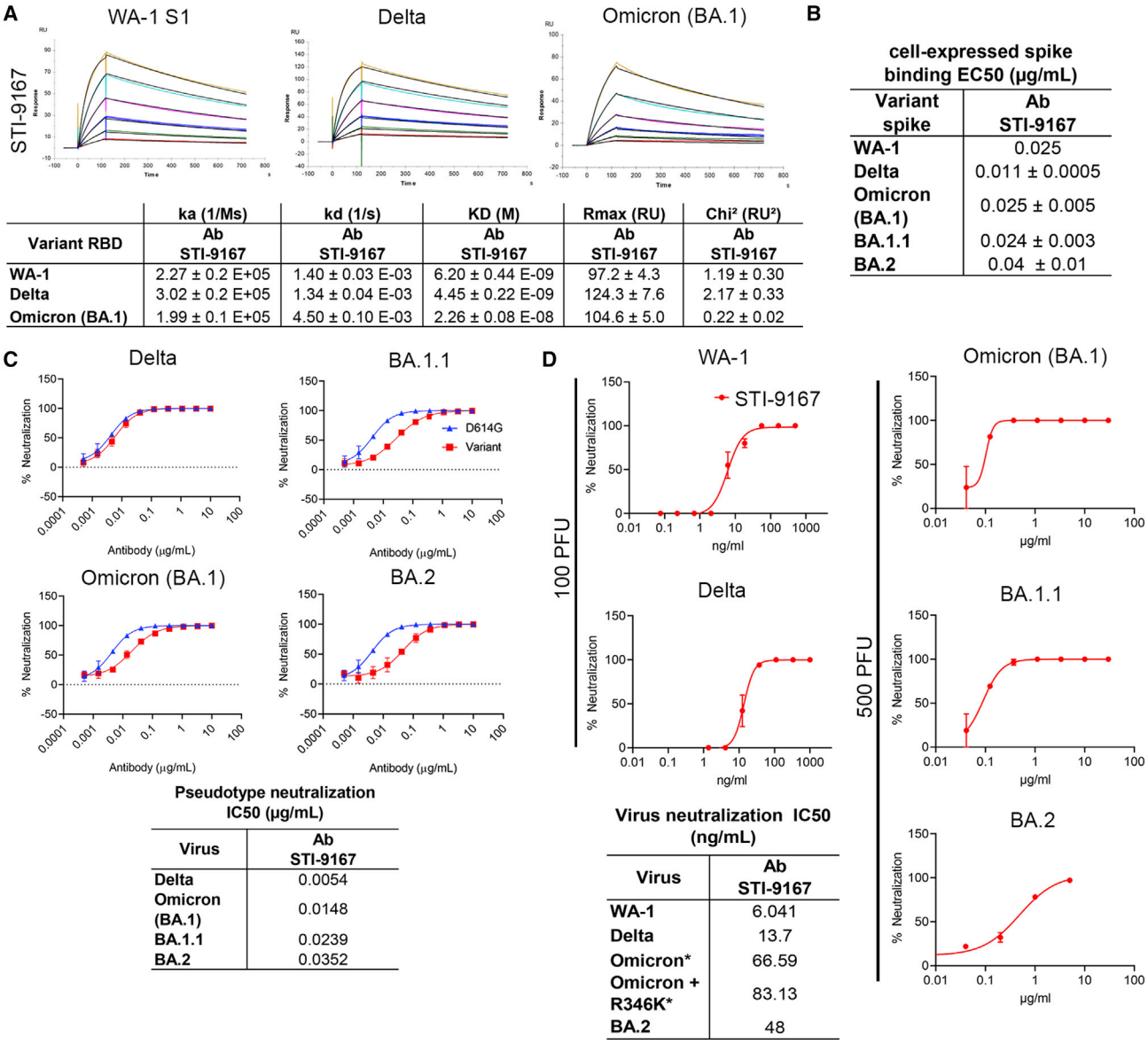

Variant RBD	ka (1/Ms) Ab STI-9167	kd (1/s) Ab STI-9167	KD (M) Ab STI-9167	Rmax (RU) Ab STI-9167	Chi² (RU²) Ab STI-9167
WA-1	2.27 ± 0.2 E+05	1.40 ± 0.03 E-03	6.20 ± 0.44 E-09	97.2 ± 4.3	1.19 ± 0.30
Delta	3.02 ± 0.2 E+05	1.34 ± 0.04 E-03	4.45 ± 0.22 E-09	124.3 ± 7.6	2.17 ± 0.33
Omicron (BA.1)	1.99 ± 0.1 E+05	4.50 ± 0.10 E-03	2.26 ± 0.08 E-08	104.6 ± 5.0	0.22 ± 0.02

cell-expressed spike binding EC50 (μg/mL)

Variant spike	Ab STI-9167
WA-1	0.025
Delta	0.011 ± 0.0005
Omicron (BA.1)	0.025 ± 0.005
BA.1.1	0.024 ± 0.003
BA.2	0.04 ± 0.01

Pseudotype neutralization IC50 (μg/mL)

Virus	Ab STI-9167
Delta	0.0054
Omicron (BA.1)	0.0148
BA.1.1	0.0239
BA.2	0.0352

Virus neutralization IC50 (ng/mL)

Virus	Ab STI-9167
WA-1	6.041
Delta	13.7
Omicron*	66.59
Omicron + R346K*	83.13
BA.2	48

Figure 2. Binding and neutralization of candidate antibody

(A) Affinity measurements of STI-9167 for spike S1 subunit binding domain from the following isolates and VOC: USA/WA-1/2020(WA-1) isolate, Delta, and Omicron. The antibody affinities were measured by SPR on a BIAcore T200 instrument using a 1:1 binding model.

(B) Spike protein derived from WA-1, Delta, Omicron, and BA.1.1 SARS-CoV-2 isolates were independently expressed on the surface of HEK293 cells. Serially diluted STI-9167 was assayed for spike protein binding by flow cytometry. To quantify antibody binding, mean fluorescent intensity was measured for each dilution tested and the EC_{50} value was calculated for each nAb. Representative replicate experiments are shown.

(C) Spike-pseudotyped VSV neutralization. The antibody neutralization curves of the indicated spike variant pseudotyped VSVs (materials and methods) are representative of three independent experiments with error bars representing one standard deviation. IC_{50} values for each pseudotype virus/antibody combination are indicated.

(D) PRNT assay using STI-9167 with SARS-CoV-2 variants (materials and methods) is presented as percent neutralization with the calculated IC_{50} values: 100 PFU was used with WA-1 and Delta, whereas 500 PFU was used for Omicron and BA.1.1, asterisks in the table indicate the higher PFU used. Values represent mean ± SD.

spike for those nAbs considered in the SPR studies followed the same pattern as that determined for spike monomer binding, with the greatest concordance in binding efficiency observed between STI-9167 and COV2-2130 (Table 2; Figure S3E). Of note, the half-maximal binding concentration of STI-9167 to the Omicron BA.1.1

Table 1. Binding of various neutralizing antibodies to SARS-CoV-2 and select VOC

Binding affinity to spike S1 Omicron (BA.1)					
Reference clone nAb	k_a (1/Ms)	k_d (1/s)	K_D (M)	R_{max} (RU)	Chi^2 (RU^2)
STI-9167	1.99 E+05 ± 1.16 E+04	4.5 E−03 ± 1.00 E−04	2.26 E−08 ± 8.50 E−10	104.6 ± 5.0	0.22 ± 0.02
COV2-2130	1.06 E+05 ± 8.05 E+04	2.28 E−02 ± 9.69 E−03	2.5 E−07 ± 7.67 E−08	59.8 ± 16.4	0.1 ± 0.05
COV2-2196	N/D	N/D	N/D	N/D	N/D
S309	1.62 E+04 ± 1.01 E+03	3.95 E−04 ± 1.53 E−05	2.45 E−08 ± 2.38 E−09	63.9 ± 7.2	0.01 ± 0.01
COV2-2130 + COV2-2196	N/D	N/D	N/D	N/D	N/D
LY-CoV1404	7.92 E+04 ± 5.92 E+03	6.77 E−03 ± 5.15 E−04	8.55 E−08 ± 2.38 E−09	179 ± 11.7	0.05 ± 0.01

N/D, not determined; RU, resonance unit. Values represent mean ± SD.
Omicron spike S1 binding affinity to indicated nAbs.

spike (EC_{50} = 0.024 μg/mL) was equivalent to that measured for Omicron BA.1, suggesting that the epitope recognized by STI-9167 is preserved in the context of BA.1.1 compared with epitopes engaged by COV2-2130, which displayed reductions in BA.1.1 spike binding of over 60-fold compared with EC_{50} values in assays targeting the Omicron BA.1 spike. Based on the spike S1 and full-length spike protein binding data, STI-9167 was further profiled to determine the potency of virus neutralization and the breadth of neutralizing protection that this antibody provided against SARS-CoV-2 VOC *in vitro*.

Pseudotyped virus particles were used to determine the neutralization potency (IC_{50}) of STI-9167 against an index virus generated with a spike protein that carries a single D614G ($VSV^{D614G\text{-}spike}$) mutation, proposed to enhance virus production, compared with the WA-1 spike protein.[36] To approximate conditions found in the setting of human SARS-CoV-2 infection, pseudotyped particle assays were carried out using HEK293 cells overexpressing human ACE2 and TMPRSS2 proteins. The average IC_{50} value for STI-9167 in assays using the $VSV^{D614G\text{-}spike}$ pseudovirus was 3.6 ng/mL (Table 3). The STI-9167 neutralization potency for $VSV^{Delta\text{-}spike}$ (IC_{50} = 5.4 ng/mL), $VSV^{Omicron\ BA.1\text{-}spike}$ (IC_{50} = 14.8 ng/mL), $VSV^{Omicron\ BA.1.1\text{-}spike}$ (IC_{50} = 23.9 ng/mL), and $VSV^{Omicron\ BA.2\text{-}spike}$ (IC_{50} = 35.2 ng/mL) pseudotyped particles was maintained to within 10-fold of that measured in assays with the $VSV^{D614G\text{-}spike}$ pseudotyped particles (Figure 2C). Furthermore, STI-9167 neutralization potency was maintained to the same degree against the full catalog of VOC-based pseudovirus tested, including Alpha, Beta, Gamma, Delta Plus, Epsilon, Zeta, Iota, Kappa, Lambda, and Mu VOC (Figure S3F). The concentrations of EUA-approved nAbs required to achieve half-maximal and 80% maximal levels of neutralization potency for VOC pseudotyped particles as well as for the $VSV^{D614G\text{-}spike}$ pseudotyped particles are detailed in Table 3. Neutralization profiling of STI-9167 was extended to include measurement of potencies against a panel of D614G spike pseudotypes. Each D614G spike pseudovirus carried one additional amino acid substitution that reflected spike mutations previously identified as a determinant of resistance to EUA-approved nAbs or as an identifying spike mutation in an emergent VOC. Substitution mutations in spike across the region spanning amino acid residues 484–489 resulted in a reduction in neutralization with the most profound effects observed for the N487Y mutation (Figure S3F). Of note, recent work has reported an approximately 10-fold reduction in ACE2 binding affinity for spike proteins encoding mutations in this same region at residue 487.[37,38] The potency of STI-9167, COV2-2130, and COV2-2196, and the COV2-2130/COV2-2196 cocktail, was further characterized in live virus neutralization assays utilizing Vero cells. Neutralizing activity was determined following infection with WA-1 strain, Delta variant, and subvariants Omicron BA.1, Omicron BA.1.1, or Omicron BA.2 and compared with EUA-approved antibodies (Figures 2D, S3G, and S3H; Table 3). In keeping with the results from

Table 2. Cell binding of various neutralizing antibodies to SARS-CoV-2 and select VOC

Cell binding			
	HEK293 cells		
	WA-1	Omicron (BA.1)	BA.1.1
Reference clone nAb	EC_{50} (μg/mL)	EC_{50} (μg/mL)	EC_{50} (μg/mL)
STI-9167	0.014	0.025	0.025
COV2-2130	0.084	0.44	27.2
COV2-2196	0.0087	1.52	0.79
COV2-2130 + COV2-2196	N/D	N/D	N/D
S309	0.6253	14.5	2.82
LY-CoV1404	0.0587	0.04	0.046

N/D, not determined.
Spike protein from selected VOC expressed on HEK293 cells binding to nAbs is expressed as EC_{50} (μg/mL).

pseudovirus assays, we observed that STI-9167 neutralized all isolates tested including the Delta variant and Omicron subvariants at half-maximal concentrations within 9-fold of those measured against live WA-1 virus, with an IC_{50} of 66.6 ng/mL against live Omicron BA.1 subvariant virus following infections with 500 PFU of each respective virus (Figure 2D). The neutralization potency for Omicron BA.1 virus in experiments using Vero target cells was 582.5 ng/mL for COV2-2130, 197.2 ng/mL for COV2-2196, 200.5 ng/mL for the COV2-2130/2196 cocktail, and 393 ng/mL for S309. Additional experiments evaluating the activity of STI-9167 against live Omicron subvariant viruses demonstrated neutralizing potencies that tracked with those measured using cognate pseudotyped virus particles, with Omicron BA.1 potency measured as 66.6 ng/mL compared with 83.1 ng/mL against Omicron BA.1.1 and 48.0 ng/mL against Omicron BA.2.

Pharmacokinetics

The biodistribution of STI-9167 was evaluated following delivery by either the i.v. or i.n. route. These studies illustrate the potential effects of delivery route on the timing of antibody exposure in the lung tissue and sera of treated mice. Following i.v. treatment at a dose level of 0.5 mg/kg, STI-9167 was detected in the serum, spleen, lungs, small intestine, and large intestine of most animals. Detected levels in the serum following i.v. dosing at the 0.5 mg/kg dose averaged 6.2 μg/mL, while STI-9167 was undetected in lung lavage material at each of the i.v. doses tested (Figure 3A). Upon processing of lung tissue, antibody was detected at a mean concentration of 0.4 ng/mg of tissue in the 0.5 mg/kg i.v. dose group. Lower i.v. doses of STI-9167 did not lead to a statistically significant difference in antibody detected in lung tissue compared with untreated animals. Antibody levels in the spleen reached an average concentration of 0.2 ng/mg of tissue within 24 h of i.v. dosing at 0.5 mg/kg. Similarly, antibody was detectable in a majority of both the small and large intestines only at the highest dose level, with average concentrations of 0.14 and 0.07 ng/mg of tissue, respectively (Figure 3A).

Following i.n. administration of STI-9167, the concentration of antibody in the serum at 24 h reached an average value of 0.054 μg/mL in the 0.5 mg/kg dose group. Compared with i.v.-treated animals at the 0.5 mg/kg dose, STI-9167 administered i.n. resulted in a 114-fold lower concentration of antibody in serum at the 24-h time point. In contrast, STI-9167 concentrations in lung lavage samples following i.n. dosing reached 0.18 μg/mL in the 0.5 mg/kg group, a 9-fold increase over lung lavage nAb levels observed following i.v. delivery of the 0.5 mg/kg dose,

Table 3. Neutralization of various neutralizing antibodies to SARS-CoV-2 and select VOC

Pseudotype neutralization							Neutralization	
	HEK-Blue 293 hACE2-TMPRSS2 cells						Vero cells	
	D614G		Omicron (BA.1)		BA.1.1		SARS-CoV-2^{WA}	SARS-CoV-2$^{omicron\ BA.1}$
Reference clone nAb	IC_{50} (μg/mL)	IC_{80} (μg/mL)	IC_{50} (μg/mL)	IC_{80} (μg/mL)	IC_{50} (μg/mL)	IC_{80} (μg/mL)	IC_{50} (ng/mL)	IC_{50} (ng/mL)
STI-9167	0.0036	0.0123	0.0148	0.0774	0.0239	0.1266	6.041	54.29
COV2-2130	0.0353	0.0783	9.105	>10	>10	>10	56.34	582.5
COV2-2196	0.0067	0.0184	0.6386	5.059	0.4696	3.55	8.726	197.2
COV2-2130 + COV2-2196	0.004	0.0108	0.0738	0.227	0.0894	0.581	N/D	200.5
S309	N/D	N/D	N/D	N/D	N/D	N/D	166.7	393
LY-CoV1404	0.0074	0.0207	0.0147	0.0523	0.0111	0.0387	N/D	10.12

N/D, not determined.
Spike-pseudotyped VSV neutralization and live virus neutralization on Vero and VERO-ACE2 cells for the WA-1 and the Omicron virus, using the indicated nAbs.

confirming that lung lavage materials can more efficiently collect drugs delivered through the airway than those delivered i.v. In lung tissue samples at 24 h following the 0.5 mg/kg i.n. dose, STI-9167 was detected at 0.173 ng/mg of tissue, similar to those levels recorded in i.v.-treated animals at the same dose level. STI-9167 levels in spleen, small, and large intestine at all i.n. dose levels tested did not rise to concentrations above background (Figure 3B).

Overall, i.n. delivery of STI-9167 led to lower serum antibody concentrations, increased lung lavage concentrations, decreased lung tissue concentration, and similar tissue concentrations in the spleen, small intestine, and large intestine when compared with i.v. delivery. Lung tissue STI-9167 concentrations were consistently higher following i.v. administration, presumably due to the fact that the lung vasculature is among the first areas where localized accumulation of i.v. administered mAbs is observed. Entry into the lung tissue and vasculature across the pulmonary mucosa following i.n. nAb administration appears to occur at a slower rate for STI-9167. Of interest, these results suggest that i.n. administration serves to increase the amount of antibody in the pulmonary lavage material over those levels that can be achieved through extravasation of antibody from the lung vasculature into the lavage material following i.v. administration, potentially allowing for more efficient neutralization of respiratory virus particles present in the extravascular spaces along the respiratory tract during the initial stages of infection.

To characterize STI-9167 pharmacokinetic parameters following i.n. dosing, antibody levels in CD-1 mouse lung tissue lysates and serum were quantified at designated time points spanning a total of 336 h using a human antibody detection ELISA (Figure 3C). In this assay, the background concentration was 16.8 ng/mL based on measurements obtained using pre-dose samples. Following i.n. administration of STI-9167, the antibody concentration was quantifiable for most of the animals at the 336 h time point in both the lungs and serum (Figure 3C). The C_{max} value of STI-9167 in the lungs was measured at 1.5 h (T_{max}) post-administration at a value of 43 μg/mL. In the lungs following i.n. administration, STI-9167 exhibited an apparent terminal half-life ($T_{1/2}$) of 26.6 h. Kinetics of STI-9167 exposure in the lungs following i.n. administration contrasted with the slower rate of antibody accumulation in the serum of treated mice (Figure 3C). Antibody was first detected in the serum at 1.5 h post-administration and the C_{max} of 456 ng/mL was reached at the 168 h time point (T_{max}), although consideration of the standard deviations in values measured among animals on or between the 72 and 168 h time points suggests that

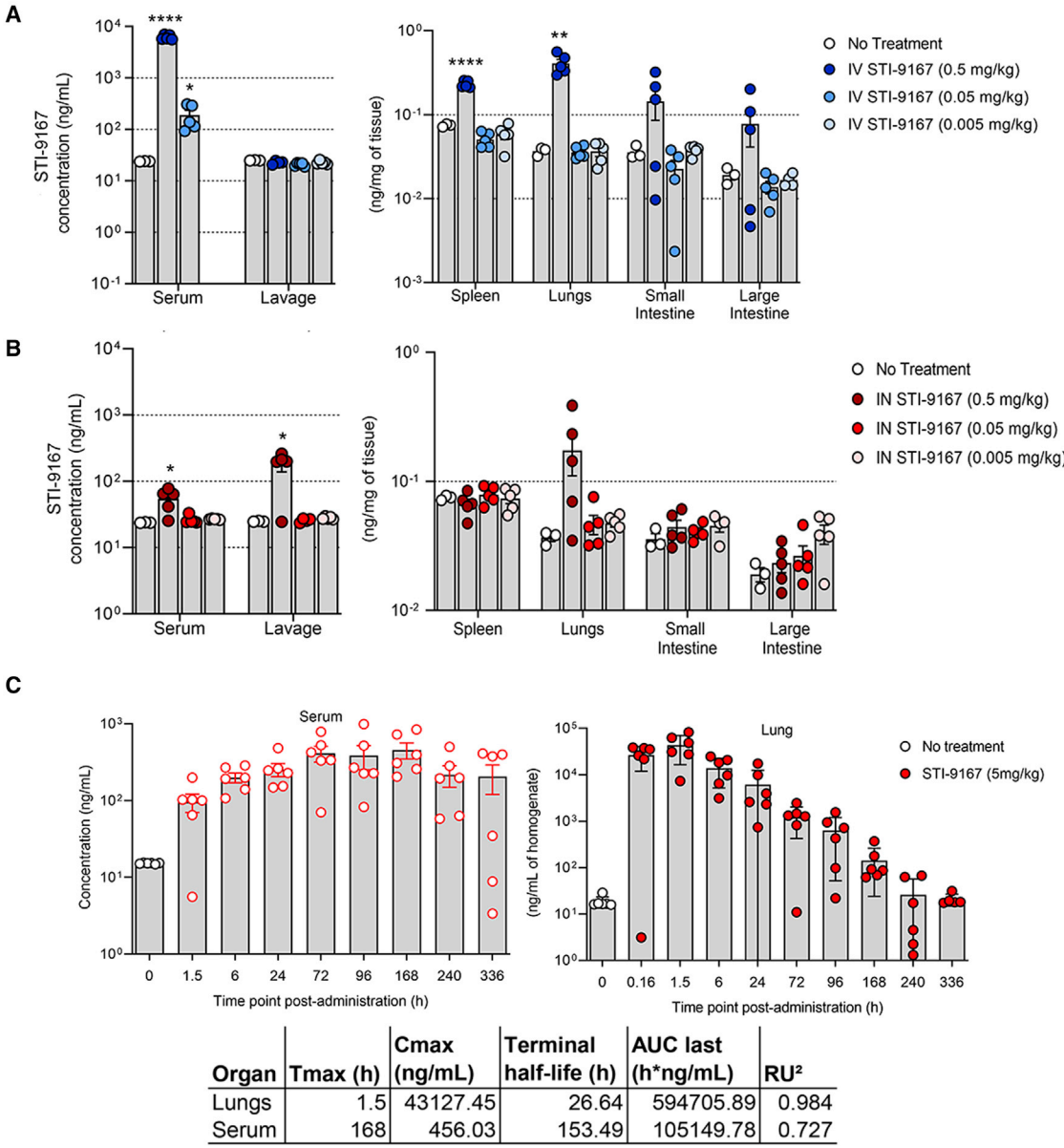

Organ	Tmax (h)	Cmax (ng/mL)	Terminal half-life (h)	AUC last (h*ng/mL)	RU²
Lungs	1.5	43127.45	26.64	594705.89	0.984
Serum	168	456.03	153.49	105149.78	0.727

Figure 3. Pharmacokinetics of neutralizing antibody

Biodistribution: concentration of STI-9167 in serum and lung lavage or lysates of spleens, lungs, small intestines, and large intestines collected from female CD-1 mice administered STI-9167 (A) i.v. at doses of 0.5 mg/kg (●), 0.05 mg/kg (●), or 0.005 mg/kg (●), or (B) i.n. at doses of 0.5 mg/kg (●), 0.05 mg/kg (●), and 0.005 mg/kg (●) at 24 h post-administration compared with samples collected from untreated mice (white circles). Values represent mean ± SEM (n = 3–4 animals in the no-treatment group, n = 5 in the treatment groups). Pharmacokinetics: concentration of STI-9167 (C) in lungs and isolated serum collected from female CD-1 mice administered STI-9167 i.n. at a dose of 5 mg/kg. Samples from treated mice were collected at the indicated time point post-administration; antibody concentrations were quantified by ELISA and compared with samples collected from untreated mice. Values represent mean ± SD (n = 3–6 animals in the no-treatment group, n = 6 per time point in the treatment groups). Significant differences are denoted by *p < 0.05, **p < 0.01, ***p < 0.001, ****p < 0.0001.

the T_{max} may have occurred as early as 72 h post-administration. Antibody levels remained relatively constant in serum over the period spanning 24–336 h, which is in keeping with the calculated STI-9167 serum half-life observed following i.v. STI-9167 administration in CD-1 mice (data not shown). The total systemic antibody exposure (AUC_{last}) was greater than 5-fold higher in the lungs than in the serum of i.n.-treated

mice (AUC_{last} values were 594,705 and 105,149 h*ng/mL, respectively), suggesting that the antibody would be effective as a potential therapeutic treatment.

Treatment using i.v.-administered STI-9167 or i.n.-administered STI-9199 in the K18-hACE2 transgenic mouse model of COVID-19

SARS-CoV-2 pathogenesis in the K18-ACE2 transgenic model of COVID-19 respiratory disease provides a tractable model to assess nAb activity in a preclinical model of respiratory disease.[39–41] The clinical signs and histological markers of pathogenesis in this model include weight loss over 5 days post-infection and the presence of microscopic lesions in the infected lungs.[40–43] Peak virus lung titers are typically detected by day 5 post-infection, but the timing and peak amplitude of replication in the lungs can vary depending on the specific VOC used to challenge the mice.[42] The breadth of protection provided by STI-9167 or STI-9199 (STI-9167 formulated for i.n. administration) was established by treating mice following virus challenge with 1×10^5 half-maximal tissue culture infectious dose ($TCID_{50}$) of the WA-1 strain, the Delta variant, or the Omicron BA.1 subvariant. Animals treated with the anti-RSV antibody, palivizumab, as the isotype control antibody lost weight in each experiment to 91.3% with the WA-1 strain, 89% with the Delta variant, and 94.7% with the Omicron BA.1 subvariant (Figures 4B–4E) compared with day 0. To determine the effects of the route of administration on the degree of protection conferred by treatment with STI-9167 (5–20 mg/kg), antibody was administered by either i.v. injection (Figure 4A) or i.n. instillation (Figure 4D). At a dose level of 5 mg/kg, administration of STI-9167 or STI-9199 to K18-hACE2 mice by the i.v. or i.n. route, respectively, provided protection against weight loss caused by the WA-1 strain, the Delta variant, and the Omicron BA.1 subvariant (Figures 4B and 4E). Virus replication in the lungs, quantified on day 4 post-infection, was approximately 2.5×10^6, 2.1×10^4, and 4.5×10^2 $TCID_{50}$/g on average in isotype control-treated mice infected with the WA-1, the Delta variant, or the Omicron BA.1 subvariant, respectively. A dose level of nAb corresponding to the level utilized in PK experiments was selected as the minimum to be administered by each route in the efficacy model. This dose was increased in 2-fold steps to account for any differences in the size or age of animals used in the PK study and the K18 ACE2 mice as well as to establish a potential dose-response relationship for any observed clinical signs in the efficacy study. Following infection by each of the SARS-CoV-2 challenge viruses, lung virus titers in mice treated with STI-9167 or STI-9199 were reduced to levels below the limit of quantification, independent of the nAb dosing route or the nAb dose level (Figures 4C and 4F). Immunohistological staining for the SARS-CoV-2 nucleocapsid demonstrated that STI-9167 and STI-9199 resulted in decreased virus burden in the lungs of infected animals treated with either route (Figure 4G). Virus infection was distributed in a predominantly peri-bronchial/bronchiolar pattern, whereas replication and spread of WA-1 was most effectively inhibited by the STIs, with some loss of potency against later variants. Of note, virus burden at the highest nAb dose level (20 mg/kg) was markedly diminished in all areas of the lung following i.n. administration of STI-9199, whereas virus burden was evident throughout the tissue sections in i.v.-treated animals at all doses. Histochemical staining of the infected lungs from each group revealed areas of dense consolidation corresponding to virus-infected areas in IHC sections (Figure S4A, green arrowheads), while the aerated/non-consolidated lung parenchyma corresponds to an absence of virus staining (Figure S4A, blue arrowheads). Collectively, STI-9167 provides protection against infection and dissemination of SARS-CoV-2 and variants.

DISCUSSION

Use of antibody discovery platforms that do not require material derived from infected individuals, such as the vaccination strategy employed here or the screening

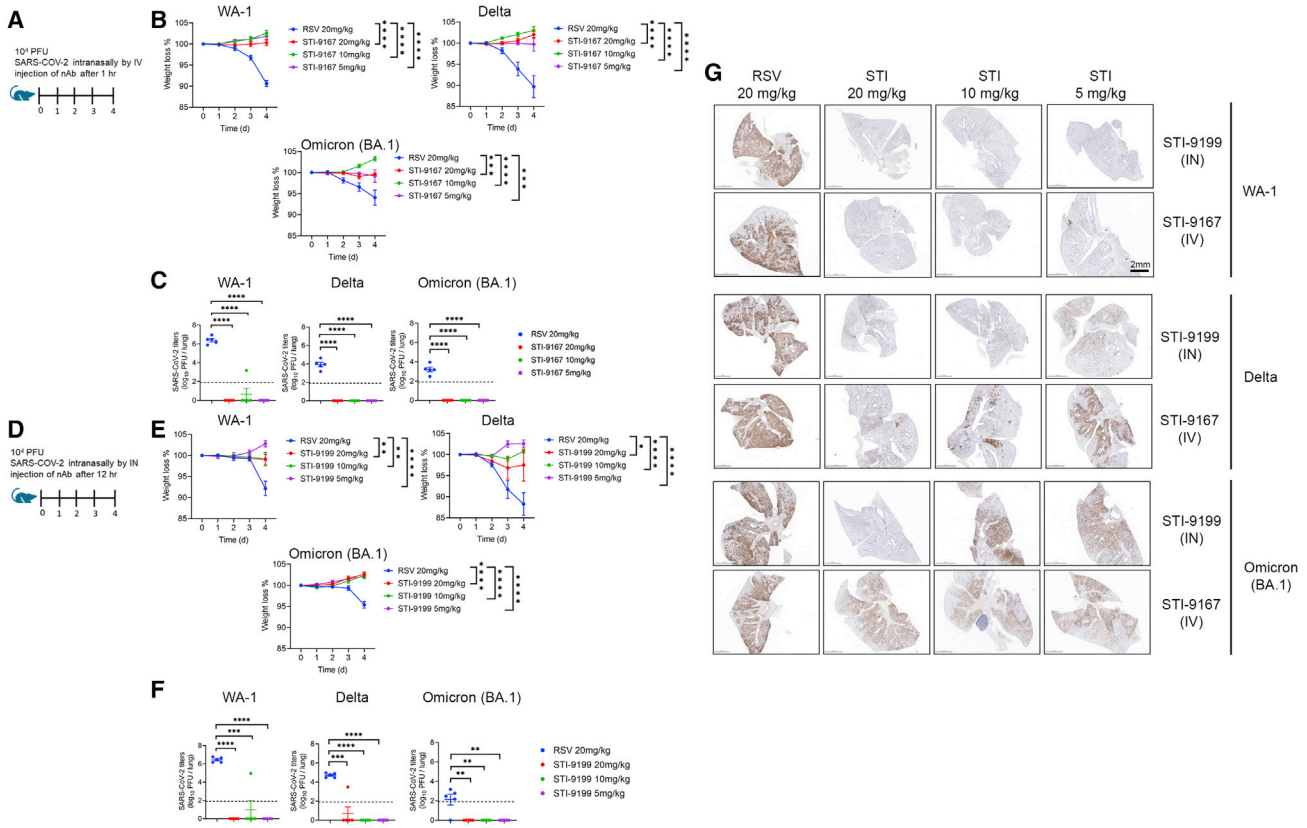

Figure 4. Efficacy of i.v. STI-9167 or i.n. delivery of STI-9199 neutralizing antibody in the K18-hACE2 murine model of COVID-19

(A) K18-hACE2 transgenic mice were infected with 10,000 PFU of WA-1, Delta, or Omicron SARS-CoV-2 and treated with the indicated concentrations of the isotype control antibody (RSV) or STI-9167 i.v. 1 h post-infection.

(B) Body weight change of mice was measured daily (n = 5).

(C) SARS-CoV-2 viral titers were measured in the lung on day 4 post-infection (n = 5).

(D) K18-hACE2 transgenic mice were infected with 10,000 PFU SARS-CoV-2 WA-1, Delta, or Omicron strains and treated with the indicated concentrations of isotype or STI-9199 intranasally at 12 h post-infection.

(E) Body weight change of mice was measured daily (n = 5).

(F) SARS-CoV-2 viral titers were measured in the lung on day 4 post-infection (n = 5). Lower limit of quantification indicated by the dashed line.

(G) Histological staining of the SARS-CoV-2 nucleocapsid (NP) antigen in lung tissue was performed for mice infected with the indicated VOC and various concentrations of STI-9167 (i.v.) or STI-9199 (i.n.) (n = 5). Representative images are shown. Scale bar, 2 mm. Values represent mean ± SEM, significant differences are denoted by *p < 0.05, **p < 0.01, ***p < 0.001, or ****p < 0.0001. Values were determined using a two-way ANOVA (B and E) and unpaired t test (C and F).

of established antibody libraries, can provide a preemptive means of addressing the challenges presented by pandemic threat pathogens.[14,44] The production of human antibodies in transgenic animals has several advantages, including *in vivo* affinity maturation, increased diversity, and clonal selection for antibody optimization.[45] Thus, the generation of antibodies to specific protein domains allows for the development of highly reactive and effective antibody therapeutics.

The pool of antibodies we identified following vaccination of mice with a SARS-CoV-2 RBD protein based on the Wuhan-1 spike protein includes a candidate with potent neutralizing activity against many SARS-CoV-2 VOC that have emerged in the past 2 years of the pandemic. Our antibody binding studies and virus neutralization assays have provided clear evidence of the broad and potent neutralizing activity of STI-9167 toward VOC identified in the early period of the pandemic as well as those currently impacting public health, including the Delta and Omicron subvariants.

Following demonstration of neutralizing activity against the Omicron BA.1 subvariant, the subvariant with the highest initial prevalence, we have extended our activity profiling studies to include assessment of the Omicron BA.1.1 and Omicron BA.2 subvariants. The frequency of Omicron BA.1.1 virus sequences rose steadily following the first reports in November of 2021 describing detection of the Omicron BA.1 variant,[46–48] and the incidence of detection of Omicron BA.2 sequences has since increased to the extent that Omicron BA.2 has become the prevalent cause of infection among newly diagnosed patients across the European subcontinent. Using a virus pseudotype (Omicron BA.1.1 and Omicron BA.2) as well as a live virus (Omicron BA.1 and BA.2), we have demonstrated STI-9167 activity against the Omicron BA.1.1 and BA.2 subvariants. In addition, we described neutralizing activity against the Mu variant pseudotype, which also encodes the R346K spike substitution.[7] The Omicron and Mu variants constitute divergent variants of SARS-CoV-2, and our studies indicate that the R346K substitution is not sufficient in either of these contexts to provide a means of resistance to the neutralizing effects of STI-9167.

Our studies of nAb STI-2020 previously demonstrated the protective efficacy of i.n.-administered antibodies in the context of SARS-CoV-2 preclinical models of pathogenesis.[49] Previous work in preclinical models of respiratory virus pathogenesis support the use of i.n.-administered IgG and IgA mAbs in prophylactic and therapeutic dosing regimens.[25,50–53] More recently, the protective effects of nAb administered i.v. or by the intramuscular route in the context of SARS-CoV-2 infection of non-human primates has been correlated with sustained nAb levels in the serum, bronchial alveolar lavage, and nasal swabs of infected animals.[54] In the current report, we demonstrate the protective effects of STI-9167 delivered by either the i.n. or the i.v. route to animals infected with the WA-1 strain, the Delta variant, or the Omicron BA.1 subvariant. As demonstrated in recently reported preclinical studies of Omicron pathogenesis, as well as our experiments, the severity of clinical signs and the amount of virus replication in the lungs following Omicron BA.1 infection was reduced in comparison with that following infection with the WA-1 strain or the Delta variant.[55–57] Independent of the challenge virus, i.n. treatment of 5 mg/kg with STI-9167 in K18 ACE2 transgenic mice at 12 h post-infection provided protection against the weight loss observed in control animals and also reduced virus lung titers to below the level of quantitation (Figures S4B–S4D). Of note, following infection by the Delta and Omicron variants, the virus burden detected by immunohistochemistry was reduced in the lungs of i.n.-treated animals compared with levels detected in the lungs of i.v.-treated animals at the same nAb dose level. The dynamics of disease onset and progression following i.n. nAb dosing indicate a potential role for i.n. nAbs administered as monotherapy or in combination with i.v. nAbs or direct-acting small molecules. These studies are consistent with the findings that i.n. delivery of antibodies against the influenza envelope hemagglutinin and neuraminidase demonstrated therapeutic protection against the influenza virus.[26,58] Phase 1 clinical studies with STI-2099 (plutavimab) have demonstrated the safety of nAb delivered as formulated liquid drops to the upper airways. A phase 2 study has completed enrollment in the US, and additional phase 2 studies are ongoing in Mexico and the United Kingdom. Based on the favorable *in vivo* potency and physicochemical profile of STI-9167, a cGMP drug product has been prepared for similar anticipated clinical studies of STI-9167 administered i.v. or as i.n. drops (STI-9199).

Virus pathogenesis in the K18 hACE2 transgenic mouse model varies depending on the specific variant used to infect the animals. In the case of animals infected with the Omicron BA.1 variant, the degree of weight loss and virus replication in the lungs was decreased compared with animals infected with either the Delta variant or the WA-1 strain. The decreased magnitude of virus replication and virus pathogenesis

in Omicron-infected animals limited the estimation of therapeutic effects following nAb treatment by either the i.v. or the i.n. route. Despite these limitations, we observed a reproducible reduction in pathogenic effects and lung virus replication for all SARS-COV-2 variants tested in the K18 hACE2 transgenic mouse model following treatment i.v. with STI-9167 or treatment i.n. with STI-9199.

STAR★METHODS

Detailed methods are provided in the online version of this paper and include the following:

- KEY RESOURCES TABLE
- RESOURCE AVAILABILITY
  - Lead contact
  - Materials availability
  - Data and code availability
- EXPERIMENTAL MODEL AND SUBJECT DETAILS
  - Animal models
  - Cell lines
- METHOD DETAILS
  - Immunizations and hybridoma generation
  - Sequencing and humanizing of antibodies
  - Formulation of STI-9199
  - Synthesis of comparison antibodies
  - Antibody characterization
  - Cell-based SARS-CoV-2 spike-binding assay
  - Cells and viruses
  - SARS-CoV-2 neutralization assay (ISMMS)
  - SARS-CoV-2 neutralization assay
  - Plasmids
  - VSV-spike pseudotype generation
  - Pseudotyped virus particle neutralization assays
  - Affinity measurements
  - Biodistribution study
  - Pharmacokinetic study
  - khACE2 mouse model of COVID-19 infection
  - Determination of infectious virus titer in the lung
  - Plaque reduction neutralizing assay
- HISTOCHEMICAL STAINING AND ANALYSIS
- QUANTIFICATION AND STATISTICAL ANALYSIS

SUPPLEMENTAL INFORMATION

Supplemental information can be found online at https://doi.org/10.1016/j.medj.2022.08.002.

ACKNOWLEDGMENTS

This work was partly supported by CRIPT (Center for Research on Influenza Pathogenesis and Transmission), an NIAID-funded Center of Excellence for Influenza research and Response (CEIRR) (contract no. 75N93021R00014 to A.G.-S., M.S., and F.K.), by DARPA grant HR0011-19-2-0020 (to A.G.-S.), and by NCI Seronet grant U54CA260560 (to A.G.-S., M.S., and F.K.). We thank R. Albrecht for support with the BSL-3 facility and procedures at the Icahn School of Medicine at Mount Sinai, NY. We thank Mary Lopez and Madhu Kumar for their dedicated work in the Center for Therapeutic Antibody Development at the Icahn school of Medicine at Mount Sinai. We would like to give a special thanks to Dr. Louise Lammers of the Mount Sinai Innovation Partners office for their help in establishing a collaboration

between Mount Sinai and Sorrento, and to Harbor BioMed for access to the H2L2 mice. S.Y. received funding from Swiss National Science Foundation (SNF) Postdoc Mobility fellowship (P400PB_199292). M.S. laboratory is supported by NIH grant R01DK130425. We would like to thank William SooHoo for his design of the graphical abstract.

AUTHOR CONTRIBUTIONS

J.A.D., H.J., H.Z., D.T., and R.A. designed the overall experiments. R.A. and L.H. had unrestricted access to all the data. K.S., C.P., N.S., D.L., C.I.P., N.D., Y.Z., X.C., L.R.-N., A.S., R.L., S.J., E.P.C., L.K., Y.F., J.D., T.K., T.M., D.M., S.O., K.A., S.K., S.Y., and T. Kehrer performed the experiments. C.P., N.S., X.C., Y.Z., H.Z., D.B., A.S., J.D., T. Kraus, T.M., D.M., B.L., S.Y., L.M., I.M., A.R., E.M., R.R., T. Kehrer, S.J., G.S., P.W., V.S., E.M.S., H.v.B., W.S., M.S., F.K., A.G.-S., N.B., J.M.C., and Y.L. performed data analyses and statistical analyses. J.T. provided support for *in vivo* efficacy experiments. L.H. and R.A. wrote the article. C.P., J.A.D., and D.T. critically reviewed the manuscript.

DECLARATION OF INTERESTS

The A.G.-S. laboratory has received research support from Pfizer, Senhwa Biosciences, Kenall Manufacturing, Avimex, Johnson & Johnson, Dynavax, 7Hills Pharma, Pharmamar, ImmunityBio, Accurius, Nanocomposix, Hexamer, N-fold LLC, Model Medicines, Atea Pharma, and Merck, outside of the reported work. A.G.-S. has consulting agreements for the following companies involving cash and/or stock: Vivaldi Biosciences, Contrafect, 7Hills Pharma, Avimex, Vaxalto, Pagoda, Accurius, Esperovax, Farmak, Applied Biological Laboratories, Pharmamar, Paratus, CureLab Oncology, CureLab Veterinary, and Pfizer, outside of the reported work. A.G.-S. is inventor on patents and patent applications on the use of antivirals and vaccines for the treatment and prevention of virus infections and cancer, owned by the Icahn School of Medicine at Mount Sinai, New York, outside of the reported work. The Icahn School of Medicine at Mount Sinai has filed patent applications relating to SARS-CoV-2 serological assays and NDV-based SARS-CoV-2 vaccines, which list F.K. as co-inventor. Mount Sinai has spun out a company, Kantaro, to market serological tests for SARS-CoV-2. F.K. has consulted for Merck and Pfizer (before 2020) and is currently consulting for Pfizer, Third Rock Ventures, Seqirus, and Avimex. The Krammer laboratory is also collaborating with Pfizer on animal models of SARS-CoV-2. Sorrento and Mount Sinai scientists are inventors on patent applications on the use of neutralizing antibodies described in these studies for the treatment and prevention of SARS-CoV-2 infections.

Received: April 4, 2022
Revised: July 7, 2022
Accepted: July 29, 2022
Published: August 8, 2022

REFERENCES

1. Zhu, N., Zhang, D., Wang, W., Li, X., Yang, B., Song, J., Zhao, X., Huang, B., Shi, W., Lu, R., et al. (2020). A novel coronavirus from patients with pneumonia in China, 2019. N. Engl. J. Med. *382*, 727–733. https://doi.org/10.1056/NEJMoa2001017.

2. Ahn, D.G., Shin, H.J., Kim, M.H., Lee, S., Kim, H.S., Myoung, J., Kim, B.T., and Kim, S.J. (2020). Current status of epidemiology, diagnosis, therapeutics, and vaccines for novel coronavirus disease 2019 (COVID-19). J. Microbiol. Biotechnol. *30*, 313–324. https://doi.org/10.4014/jmb.2003.03011.

3. Amanat, F., and Krammer, F. (2020). SARS-CoV-2 vaccines: status report. Immunity *52*, 583–589. https://doi.org/10.1016/j.immuni.2020.03.007.

4. Mascola, J.R., Graham, B.S., and Fauci, A.S. (2021). SARS-CoV-2 viral variants—tackling a moving target. JAMA *325*, 1261–1262. https://doi.org/10.1001/jama.2021.2088.

5. Hoffmann, M., Krüger, N., Schulz, S., Cossmann, A., Rocha, C., Kempf, A., Nehlmeier, I., Graichen, L., Moldenhauer, A.S., Winkler, M.S., et al. (2022). The Omicron variant is highly resistant against antibody-mediated

neutralization: implications for control of the COVID-19 pandemic. Cell *185*, 447–456.e11. https://doi.org/10.1016/j.cell.2021.12.032.

6. Bedford, J., Enria, D., Giesecke, J., Heymann, D.L., Ihekweazu, C., Kobinger, G., Lane, H.C., Memish, Z., Oh, M.D., Sall, A.A., et al. (2020). COVID-19: towards controlling of a pandemic. Lancet *395*, 1015–1018. https://doi.org/10.1073/pnas.88.18.7978.

7. Uriu, K., Kimura, I., Shirakawa, K., Takaori-Kondo, A., Nakada, T.A., Kaneda, A., Nakagawa, S., and Sato, K.; Genotype to Phenotype Japan G2P-Japan Consortium (2021). Neutralization of the SARS-CoV-2 Mu variant by convalescent and vaccine serum. N. Engl. J. Med. *385*, 2397–2399. https://doi.org/10.1056/NEJMc2114706.

8. Cameroni, E., Saliba, C., Bowen, J.E., Rosen, L.E., Culap, K., Pinto, D., VanBlargan, L.A., De Marco, A., Zepeda, S.K., Iulio, J.d., et al. (2021). Broadly neutralizing antibodies overcome SARS-CoV-2 Omicron antigenic shift. Preprint at bioRxiv. https://doi.org/10.1101/2021.12.12.472269.

9. Aggarwal, A., Stella, A.O., Walker, G., Akerman, A., Milogiannakis, V., Brilot, F., Amatayakul-Chantler, S., Roth, N., Coppola, G., Schofield, P., et al. (2021). SARS-CoV-2 Omicron: evasion of potent humoral responses and resistance to clinical immunotherapeutics relative to viral variants of concern. Preprint at medRxiv. https://doi.org/10.1101/2021.12.14.21267772.

10. Planas, D., Saunders, N., Maes, P., Guivel-Benhassine, F., Planchais, C., Buchrieser, J., Bolland, W.H., Porrot, F., Staropoli, I., Lemoine, F., et al. (2021). Considerable escape of SARS-CoV-2 variant Omicron to antibody neutralization. Preprint at bioRxiv. https://doi.org/10.1101/2021.12.14.472630.

11. Cao, Y., Wang, J., Jian, F., Xiao, T., Song, W., Yisimayi, A., Huang, W., Li, Q., Wang, P., An, R., et al. (2021). Omicron escapes the majority of existing SARS-CoV-2 neutralizing antibodies. Preprint at bioRxiv. https://doi.org/10.1101/2021.12.07.470392.

12. Liu, L., Iketani, S., Guo, Y., Chan, J.F.W., Wang, M., Liu, L., Luo, Y., Chu, H., Huang, Y., Nair, M.S., et al. (2021). Striking antibody evasion manifested by the omicron variant of SARS-CoV-2. Preprint at bioRxiv. https://doi.org/10.1101/2021.12.14.472719.

13. VanBlargan, L.A., Errico, J.M., Halfmann, P.J., Zost, S.J., Crowe, J.E., Purcell, L.A., Kawaoka, Y., Corti, D., Fremont, D.H., and Diamond, M.S. (2021). An infectious SARS-CoV-2 B.1.1.529 Omicron virus escapes neutralization by several therapeutic monoclonal antibodies. Preprint at bioRxiv. https://doi.org/10.1101/2021.12.15.472828.

14. Cao, X., Maruyama, J., Zhou, H., Kerwin, L., Sattler, R., Manning, J.T., Johnson, S., Richards, S., Blair, B., Du, N., et al. (2020). Discovery and development of human SARS-CoV-2 neutralizing antibodies using an unbiased phage display library approach. Preprint at bioRxiv. https://doi.org/10.1101/2020.09.27.316174.

15. Elbe, S., and Buckland-Merrett, G. (2017). Data, disease and diplomacy: GISAID's innovative contribution to global health. Glob. Chall. *1*, 33–46. https://doi.org/10.1002/gch2.1018.

16. Julia L. Mullen, G. T., A. Abdel Latif, M. Alkuzweny, M. Cano, E. Haag, J. Zhou, M. Zeller, E. Hufbauer, N. Matteson, et al. (2020). https://outbreak.info/

17. Iketani, S., Liu, L., Guo, Y., Liu, L., Chan, J.F.W., Huang, Y., Wang, M., Luo, Y., Yu, J., Chu, H., et al. (2022). Antibody evasion properties of SARS-CoV-2 Omicron sublineages. Nature *604*, 553–556. https://doi.org/10.1038/s41586-022-04594-4.

18. Poh, C.M., Carissimo, G., Wang, B., Amrun, S.N., Lee, C.Y.P., Chee, R.S.L., Fong, S.W., Yeo, N.K.W., Lee, W.H., Torres-Ruesta, A., et al. (2020). Two linear epitopes on the SARS-CoV-2 spike protein that elicit neutralising antibodies in COVID-19 patients. Nat. Commun. *11*, 2806. https://doi.org/10.1038/s41467-020-16638-2.

19. Gupta, A., Gonzalez-Rojas, Y., Juarez, E., Crespo Casal, M., Moya, J., Falci, D.R., Sarkis, E., Solis, J., Zheng, H., Scott, N., et al. (2021). Early treatment for Covid-19 with SARS-CoV-2 neutralizing antibody sotrovimab. N. Engl. J. Med. *385*, 1941–1950. https://doi.org/10.1056/NEJMoa2107934.

20. Pinto, D., Park, Y.J., Beltramello, M., Walls, A.C., Tortorici, M.A., Bianchi, S., Jaconi, S., Culap, K., Zatta, F., De Marco, A., et al. (2020). Cross-neutralization of SARS-CoV-2 by a human monoclonal SARS-CoV antibody. Nature *583*, 290–295. https://doi.org/10.1038/s41586-020-2349-y.

21. Shi, R., Shan, C., Duan, X., Chen, Z., Liu, P., Song, J., Song, T., Bi, X., Han, C., Wu, L., et al. (2020). A human neutralizing antibody targets the receptor-binding site of SARS-CoV-2. Nature *584*, 120–124. https://doi.org/10.1038/s41586-020-2381-y.

22. Westendorf, K., Žentelis, S., Wang, L., Foster, D., Vaillancourt, P., Wiggin, M., Lovett, E., van der Lee, R., Hendle, J., Pustilnik, A., et al. (2022). LY-CoV1404 (bebtelovimab) potently neutralizes SARS-CoV-2 variants. Preprint at bioRxiv. https://doi.org/10.1101/2021.04.30.442182.

23. Weinreich, D.M., Sivapalasingam, S., Norton, T., Ali, S., Gao, H., Bhore, R., Musser, B.J., Soo, Y., Rofail, D., Im, J., et al. (2021). REGN-COV2, a neutralizing antibody cocktail, in outpatients with Covid-19. N. Engl. J. Med. *384*, 238–251. https://doi.org/10.1056/NEJMoa2035002.

24. Weltzin, R., and Monath, T.P. (1999). Intranasal antibody prophylaxis for protection against viral disease. Clin. Microbiol. Rev. *12*, 383–393. https://doi.org/10.1128/CMR.12.3.383.

25. Piepenbrink, M.S., Park, J.G., Oladunni, F.S., Deshpande, A., Basu, M., Sarkar, S., Loos, A., Woo, J., Lovalenti, P., Sloan, D., et al. (2021). Therapeutic activity of an inhaled potent SARS-CoV-2 neutralizing human monoclonal antibody in hamsters. Cell Rep. Med. *2*, 100218. https://doi.org/10.1038/s41467-020-15562-9 (2021.

26. Leyva-Grado, V.H., Tan, G.S., Leon, P.E., Yondola, M., and Palese, P. (2015). Direct administration in the respiratory tract improves efficacy of broadly neutralizing anti-influenza virus monoclonal antibodies. Antimicrob. Agents Chemother. *59*, 4162–4172. https://doi.org/10.1128/aac.00290-15.

27. Gardner, T.J., Stein, K.R., Duty, J.A., Schwarz, T.M., Noriega, V.M., Kraus, T., Moran, T.M., and Tortorella, D. (2016). Functional screening for anti-CMV biologics identifies a broadly neutralizing epitope of an essential envelope protein. Nat. Commun. *7*, 13627. https://doi.org/10.1038/ncomms13627.

28. Ikegame, S., Siddiquey, M.N.A., Hung, C.T., Haas, G., Brambilla, L., Oguntuyo, K.Y., Kowdle, S., Chiu, H.P., Stevens, C.S., Vilardo, A.E., et al. (2021). Neutralizing activity of Sputnik V vaccine sera against SARS-CoV-2 variants. Nat. Commun. *12*, 4598. https://doi.org/10.1038/s41467-021-24909-9 (2021.

29. Lee, W.S., Wheatley, A.K., Kent, S.J., and DeKosky, B.J. (2020). Antibody-dependent enhancement and SARS-CoV-2 vaccines and therapies. Nat. Microbiol. *5*, 1185–1191. https://doi.org/10.1038/s41564-020-00789-5.

30. Wen, J., Cheng, Y., Ling, R., Dai, Y., Huang, B., Huang, W., Zhang, S., and Jiang, Y. (2020). Antibody-dependent enhancement of coronavirus. Int. J. Infect. Dis. *100*, 483–489. https://doi.org/10.1016/j.ijid.2020.09.015.

31. Schlothauer, T., Herter, S., Koller, C.F., Grau-Richards, S., Steinhart, V., Spick, C., Kubbies, M., Klein, C., Umaña, P., and Mössner, E. (2016). Novel human IgG1 and IgG4 Fc-engineered antibodies with completely abolished immune effector functions. Protein Eng. Des. Sel. *29*, 457–466. https://doi.org/10.1093/protein/gzw040.

32. Li, D., Edwards, R.J., Manne, K., Martinez, D.R., Schäfer, A., Alam, S.M., Wiehe, K., Lu, X., Parks, R., Sutherland, L.L., et al. (2021). In vitro and in vivo functions of SARS-CoV-2 infection-enhancing and neutralizing antibodies. Cell *184*, 4203–4219.e32. https://doi.org/10.1128/aac.00290-15.

33. Donoghue, M., Hsieh, F., Baronas, E., Godbout, K., Gosselin, M., Stagliano, N., Donovan, M., Woolf, B., Robison, K., Jeyaseelan, R., et al. (2000). A novel angiotensin-converting enzyme-related carboxypeptidase (ACE2) converts angiotensin I to angiotensin 1-9. Circ. Res. *87*, E1–E9. https://doi.org/10.1161/01.res.87.5.e1.

34. Hamming, I., Timens, W., Bulthuis, M.L.C., Lely, A.T., Navis, G.J., and van Goor, H. (2004). Tissue distribution of ACE2 protein, the functional receptor for SARS coronavirus. A first step in understanding SARS pathogenesis. J. Pathol. *203*, 631–637. https://doi.org/10.1002/path.1570.

35. Harmer, D., Gilbert, M., Borman, R., and Clark, K.L. (2002). Quantitative mRNA expression profiling of ACE 2, a novel homologue of angiotensin converting enzyme. FEBS Lett. *532*, 107–110. https://doi.org/10.1016/s0014-5793(02)03640-2.

36. Korber, B., Fischer, W.M., Gnanakaran, S., Yoon, H., Theiler, J., Abfalterer, W., Hengartner, N., Giorgi, E.E., Bhattacharya, T., Foley, B., et al. (2020). Tracking changes in SARS-CoV-2 spike: evidence that D614G increases infectivity of the COVID-19 virus. Cell *182*, 812–827.e19. https://doi.org/10.1038/s41577-020-00434-6.

37. Cao, Y., Yisimayi, A., Jian, F., Song, W., Xiao, T., Wang, L., Du, S., Wang, J., Li, Q., Chen, X., et al. (2022). BA.2.12.1, BA.4 and BA.5 escape antibodies elicited by Omicron infection. Preprint at bioRxiv. https://doi.org/10.1101/2022.04.30.489997.

38. Wang, Q., Guo, Y., Iketani, S., Li, Z., Mohri, H., Wang, M., Yu, J., Bowen, A.D., Chang, J.Y., Shah, J.G., et al. (2022). SARS-CoV-2 Omicron BA.2.12.1, BA.4, and BA.5 subvariants evolved to extend antibody evasion. Preprint at bioRxiv. https://doi.org/10.1101/2022.05.26.493517.

39. Muñoz-Fontela, C., Dowling, W.E., Funnell, S.G.P., Gsell, P.S., Riveros-Balta, A.X., Albrecht, R.A., Andersen, H., Baric, R.S., Carroll, M.W., Cavaleri, M., et al. (2020). Animal models for COVID-19. Nature *586*, 509–515. https://doi.org/10.1038/s41586-020-2787-6.

40. Arce, V.M., and Costoya, J.A. (2021). SARS-CoV-2 infection in K18-ACE2 transgenic mice replicates human pulmonary disease in COVID-19. Cell. Mol. Immunol. *18*, 513–514. https://doi.org/10.1038/s41423-020-00616-1 (2021.

41. Winkler, E.S., Bailey, A.L., Kafai, N.M., Nair, S., McCune, B.T., Yu, J., Fox, J.M., Chen, R.E., Earnest, J.T., Keeler, S.P., et al. (2020). SARS-CoV-2 infection of human ACE2-transgenic mice causes severe lung inflammation and impaired function. Nat. Immunol. *21*, 1327–1335. https://doi.org/10.1038/s41590-020-0778-2.

42. Radvak, P., Kwon, H.J., Kosikova, M., Ortega-Rodriguez, U., Xiang, R., Phue, J.N., Shen, R.F., Rozzelle, J., Kapoor, N., Rabara, T., et al. (2021). SARS-CoV-2 B.1.1.7 (alpha) and B.1.351 (beta) variants induce pathogenic patterns in K18-hACE2 transgenic mice distinct from early strains. Nat. Commun. *12*, 6559. https://doi.org/10.1038/s41467-021-26803-w (2021.

43. Yinda, C.K., Port, J.R., Bushmaker, T., Offei Owusu, I., Purushotham, J.N., Avanzato, V.A., Fischer, R.J., Schulz, J.E., Holbrook, M.G., Hebner, M.J., et al. (2021). K18-hACE2 mice develop respiratory disease resembling severe COVID-19. PLoS Pathog. *17*, e1009195. https://doi.org/10.1371/journal.ppat.1009195.

44. Hansen, J., Baum, A., Pascal, K.E., Russo, V., Giordano, S., Wloga, E., Fulton, B.O., Yan, Y., Koon, K., Patel, K., et al. (2020). Studies in humanized mice and convalescent humans yield a SARS-CoV-2 antibody cocktail. Science *369*, 1010–1014. https://doi.org/10.1126/science.abd0827.

45. Lu, R.M., Hwang, Y.C., Liu, I.J., Lee, C.C., Tsai, H.Z., Li, H.J., and Wu, H.C. (2020). Development of therapeutic antibodies for the treatment of diseases. J. Biomed. Sci. *27*, 1. https://doi.org/10.1186/s12929-019-0592-z.

46. Scott, L., Hsiao, N.Y., Moyo, S., Singh, L., Tegally, H., Dor, G., Maes, P., Pybus, O.G., Kraemer, M.U.G., Semenova, E., et al. (2021). Track Omicron's spread with molecular data. Science *374*, 1454–1455. https://doi.org/10.1126/science.abn4543.

47. Hadfield, J., Megill, C., Bell, S.M., Huddleston, J., Potter, B., Callender, C., Sagulenko, P., Bedford, T., and Neher, R.A. (2018). Nextstrain: real-time tracking of pathogen evolution. Bioinformatics *34*, 4121–4123. https://doi.org/10.1093/bioinformatics/bty407.

48. Pulliam, J.R.C., van Schalkwyk, C., Govender, N., Gottberg, A.V., Cohen, C., Groome, M.J., Dushoff, J., Mlisana, K., and Moultrie, H. (2021). Increased risk of SARS-CoV-2 reinfection associated with emergence of the Omicron variant in South Africa. Preprint at medRxiv. https://doi.org/10.1101/2021.11.11.21266068.

49. Fu, Y., Maruyama, J., Singh, A., Lim, R., Ledesma, A., Lee, D., Rivero-Nava, L., Ko, J., Rivera, I., Sattler, R.A., et al. (2020). Protective effects of STI-2020 antibody delivered post-infection by the intranasal or intravenous route in a Syrian golden hamster COVID-19 model. Preprint at bioRxiv. https://doi.org/10.1101/2020.10.28.359836.

50. Halwe, S., Kupke, A., Vanshylla, K., Liberta, F., Gruell, H., Zehner, M., Rohde, C., Krähling, V., Gellhorn Serra, M., Kreer, C., et al. (2021). Intranasal administration of a monoclonal neutralizing antibody protects mice against SARS-CoV-2 infection. Viruses *13*, 1498.

51. Weltzin, R., Hsu, S.A., Mittler, E.S., Georgakopoulos, K., and Monath, T.P. (1994). Intranasal monoclonal immunoglobulin A against respiratory syncytial virus protects against upper and lower respiratory tract infections in mice. Antimicrob. Agents Chemother. *38*, 2785–2791. https://doi.org/10.1128/aac.38.12.2785.

52. Weltzin, R., Traina-Dorge, V., Soike, K., Zhang, J.Y., Mack, P., Soman, G., Drabik, G., and Monath, T.P. (1996). Intranasal monoclonal IgA antibody to respiratory syncytial virus protects rhesus monkeys against upper and lower respiratory tract infection. J. Infect. Dis. *174*, 256–261. https://doi.org/10.1093/infdis/174.2.256.

53. Zhang, H., Yang, Z., Xiang, J., Cui, Z., Liu, J., and Liu, C. (2020). Intranasal administration of SARS-CoV-2 neutralizing human antibody prevents infection in mice. Preprint at bioRxiv. https://doi.org/10.1101/2020.12.08.416677.

54. Cobb, R.R., Nkolola, J., Gilchuk, P., Chandrashekar, A., Yu, J., House, R.V., Earnhart, C.G., Dorsey, N.M., Hopkins, S.A., Snow, D.M., et al. (2022). A combination of two human neutralizing antibodies prevents SARS-CoV-2 infection in cynomolgus macaques. Med *3*, 188–203.e4. https://doi.org/10.1016/j.medj.2022.01.004.

55. Abdelnabi, R., Foo, C.S., Zhang, X., Lemmens, V., Maes, P., Slechten, B., Raymenants, J., André, E., Weynand, B., Dallemier, K., and Neyts, J. (2021). The omicron (B.1.1.529) SARS-CoV-2 variant of concern does not readily infect Syrian hamsters. Preprint at bioRxiv. https://doi.org/10.1101/2021.12.24.474086.

56. McMahan, K., Giffin, V., Tostanoski, L.H., Chung, B., Siamatu, M., Suthar, M.S., Halfmann, P., Kawaoka, Y., Piedra-Mora, C., Martinot, A.J., et al. (2022). Reduced pathogenicity of the SARS-CoV-2 omicron variant in hamsters. Preprint at bioRxiv. https://doi.org/10.1101/2022.01.02.474743.

57. Diamond, M., Halfmann, P., Maemura, T., Iwatsuki-Horimoto, K., Iida, S., Kiso, M., Scheaffer, S., Darling, T., Joshi, A., Loeber, S., et al. (2021). The SARS-CoV-2 B.1.1.529 Omicron virus causes attenuated infection and disease in mice and hamsters. Res. Sq. https://doi.org/10.21203/rs.3.rs-1211792/v1.

58. Tan, J., O'Dell, G., Hernandez, M.M., Sordillo, E.M., Kahn, Z., Kriti, D., van Bakel, H., Ellebedy, A.H., Wilson, P.C., Simon, V., et al. (2022). Human anti-neuraminidase antibodies reduce airborne transmission of clinical influenza virus isolates in the Guinea pig model. J. Virol. *96*, e0142121. https://doi.org/10.1128/jvi.01421-21.

59. Widjaja, I., Wang, C., van Haperen, R., Gutiérrez-Álvarez, J., van Dieren, B., Okba, N.M.A., Raj, V.S., Li, W., Fernandez-Delgado, R., Grosveld, F., et al. (2019). Towards a solution to MERS: protective human monoclonal antibodies targeting different domains and functions of the MERS-coronavirus spike glycoprotein. Emerg. Microbes Infect. *8*, 516–530. https://doi.org/10.1080/22221751.2019.1597644.

60. Ramakrishnan, M.A. (2016). Determination of 50% endpoint titer using a simple formula. World J. Virol. *5*, 85–86. https://doi.org/10.5501/wjv.v5.i2.85.

STAR★METHODS

KEY RESOURCES TABLE

REAGENT or RESOURCE	SOURCE	IDENTIFIER
Antibodies		
goat anti-rat (heavy chain specific) APC detection antibody	Jackson ImmunoResearch	112-136-071; RRID:AB_2338217
goat anti-rat IgG (heavy chain specific)-HRP	Jackson ImmunoResearch	112-035-008 RRID:AB_2338130
APC AffiniPure F(ab') Fragment (Goat Anti-Human IgG (H+L)	Jackson ImmunoResearch	Cat# 109-136-4098
mouse monoclonal anti-SARS2-CoV2 NP 1c7c7	Sigma Aldrich	ZMS1075 RRID:AB_2893327
anti-SARS-CoV-2 spike S2 monoclonal antibody	Sinobiological	40590-D001 RRID:AB_2857932
anti-VSV-G clone 8G5F11	Millipore	Millipore #MABF2337
STI-9167/STI-9199	In paper	N/A
Palivizumab	In paper	N/A
Bacterial and virus strains		
Wuhan seafood market pneumonia virus isolate	GenBank	GenBank Accession# MN908947
VsV-SARS-CoV-2-spike GFP-expressing reporter virus ($VsV^{CoV2\text{-}spike}$)	This Paper	N/A
SARS-CoV-2 USA/WA-1/2020 isolates	The World Reference Center for Emerging Viruses and Arboviruses (WRCEVA) at the University of Texas Medical Branch	https://www.utmb.edu/wrceva/home
USA/CA-CDC5574/2020 isolates	The World Reference Center for Emerging Viruses and Arboviruses (WRCEVA) at the University of Texas Medical Branch	https://www.utmb.edu/wrceva/home
MD-HP01542/2021 isolates	The World Reference Center for Emerging Viruses and Arboviruses (WRCEVA) at the University of Texas Medical Branch	https://www.utmb.edu/wrceva/home
202001 isolates	The World Reference Center for Emerging Viruses and Arboviruses (WRCEVA) at the University of Texas Medical Branch	https://www.utmb.edu/wrceva/home
Washington strain NR-52281; Alpha variant NR-54000; Beta Variant NR-54009; Gamma variant NR-54982; Delta variant NR- 55611 or NR-55672; Lambda variant NR- 55654: Omicron Variant NR-65461	BEI Resources	https://www.beiresources.org/Collection/56/SARS-CoV-2.aspx?f_instockflag=In+Stock%23~%23Discontinued%23~%23Temporarily+Out+of+Stock
Chemicals, peptides, and recombinant proteins		
G-Pseudotyped ΔG-luciferase (G*ΔG-luciferase) rVSV	Kerafast	Kerafast #EH1025-PM
Critical commercial assays		
SMARTer 5′ RACE technology	Takara Bio USA	https://www.takarabio.com/documents/User%20Manual/SMARTer/SMARTer%20RACE%205%273%27%20Kit%20User%20Manual.pdf
Qiagen RNeasy Mini Kit	Qiagen, Valencia, CA	Cat. No. / ID: 74004
V-Quest		http://imgt.org
Hamster: CHO-S Cells (cGMP banked) and Media Kit	ThermoFisher	A1155701
HEK293 transfection	Promega	E2311
ONE-Glo	Promega	E6110
Amaxa Nucleofector II with cell line kit L	Lonza	Lonza #VCA-1005
Deposited data		
Raw and analyzed data	This paper	N/A
Experimental models: Cell lines		
Human: Expi293F cells	Thermo Fisher	A14527: Expi293F cells; RRID:CVCL_D615
Human: HEK-293 cells	ATCC	CRL-1573; RRID:CVCL_0045
Hamster: CHO cells	ThermoFisher	A1155701; RRID:CVCL_EG60

(*Continued on next page*)

Continued

REAGENT or RESOURCE	SOURCE	IDENTIFIER
Monkey: Vero E6 cells	ATCC	CRL-1586; RRID:CVCL_0574
Hamster: Baby hamster kidney 21 (BHK21) cells	ATCC	CCL-10; RRID:CVCL_1915
HEK-Blue 293 hACE2-TMPRSS2 cells	Invivogen	Invivogen #hkb-hace2tpsa
Experimental models: Organisms/strains		
Harbour *H2L2*® human antibody transgenic mice	Harbour BioMed, Cambridge, MA	*H2L2*®
Female CD-1-IGS mice	Charles River	Strain code #022
Female K18-hACE2 transgenic mice	Jackson laboratory	Strain #:034860
Oligonucleotides		
Rat_G1_G2b_GSP1: 5′- GGCTCAGGGAAATAGCCCTTGA-3′	Takara Bio USA	Rat_G1_G2b_GSP1
Rat_G2c_GSP1: 5′-GGCTCAGGGAAATAGCCTTTGA-3′	Takara Bio USA	Rat_G2c_GSP1
Rat_cK_GSP1: 5′-GTAACACTGTCCAGGACACCATC-3′	Takara Bio USA	Rat_cK_GSP1
Recombinant DNA		
pcDNA vectors	Genscript USA Inc., Piscataway, NJ	N/A
plasmid pCDNA3.1	ThermoFisher	ThermoFisher #V79020
Software and algorithms		
FlowJo	Tree Star, Inc.	N/A
GraphPad	Prism	N/A
BIAcore T200 Evaluation software 3.1	BIAcore	N/A
Other		
ClonalCell HY-PEG	StemCell Technologies	ClonalCell HY-PEG
Lipofectamine 3000	Thermo Fisher	L3000001
Immulon 4 HBX high binding clear flat bottom 96 well plates	Thermo Fisher	3855
Biotek ELX405 MultiPlate Washer	Biotek, Winooski, VT	N/A
ABTS substrate solution	ThermoFisher	37615
sera free hybridoma media	Invitrogen	N/A
Octet Red 96 BLI Instrument	SartoriusAG, Goettingen, Germany	https://www.sartorius.com/download/552460/octet-red96e-system-datasheet-en-sartorius-data.pdf
Biacore T200 surface plasmon resonance	GE Healthcare	N/A

RESOURCE AVAILABILITY

Lead contact

Further information and requests for resources and reagents should be directed to the lead contact, Henry Ji (hji@sorrentotherapeutics.com).

Materials availability

Antibody can be made available from the lead contact upon request.

Data and code availability

- All data reported in this paper can be shared by the lead contact upon request.
- No original code is reported in this paper.
- Any additional information required to reanalyze the data reported in this paper is available from the lead contact upon request.

EXPERIMENTAL MODEL AND SUBJECT DETAILS

Animal models

Female K18-hACE2 transgenic mice were purchased from Jackson laboratory and maintained in pathogen-free conditions and handling conforms to the requirements of the National Institutes of Health and the Scripps Research Institute Animal Research Committee. Harbor *H2L2* human antibody transgenic mice (Harbor BioMed, Cambridge, MA) were utilized under a collaboration between the Icahn

School of Medicine at Mount Sinai and Harbor BioMed. Eight-to twelve-week old mice were used. Animal studies were approved by the Icahn School of Medicine Institutional Animal Care and Use Committee (IACUC). Female CD-1-IGS mice (strain code #022) were obtained from Charles River at 6–8 weeks of age with a weight range of 22–28.8 g. Animal experiments were approved by Sorrento Therapeutics, Inc. Protocol approval committee and IACUC.

Cell lines

Expi293F cells are maintained in Expi293 Expression Medium at 37°C. CHO-S cells in exponential phase at a cell density of 10^6 cells/mL with viability of ≥93%, were co-transfected for antibody expression at 37°C. HEK293 cells were transfected using FuGeneHD transfection reagent according to manufacturer's protocol (Promega, Cat #E2311) at at 37°C. Baby hamster kidney 21 (BHK21) cells (ATCC #CCL-10) were maintained in DMEM/F12 media (Thermo Fisher #21041025) supplemented with 10% fetal bovine serum (Omega Scientific #FB-02) and 5% tryptose phosphate broth (Thermo Fisher #18050039). BHK21/WI-2 cells (Kerafast #EH1011) were maintained in DMEM (Thermo Fisher #11965092) supplemented with 5% fetal bovine serum at 37°C. 293-ACE2 cells were maintained in DMEM supplemented with 10% fetal bovine serum and 200 μg/mL G418 (Invivogen #ant-gn-2) at 37°C. HEK-Blue 293 hACE2-TMPRSS2 cells (Invivogen #hkb-hace2tpsa) were maintained in DMEM supplemented with 10% fetal bovine serum, 0.5 μg/mL puromycin (Invivogen #ant-pr-1), 200 μg/mL hygromycin-B (Invivogen #ant-hg-1), and 100 μg/mL zeocin (Invivogen #ant-zn-1) at 37°C. VeroE6 cells were plated at 18.0E+03 cells/well for SARS-CoV-2 were maintained in DMEM medium (GIBCO) supplemented with 2% FBS (PAN Biotech), 1% Penicillin Streptomycin (GIBCO) and 1% HEPES (GIBCO) at 37°C.

METHOD DETAILS

Immunizations and hybridoma generation

To generate human antibodies, Harbor *H2L2*® human antibody transgenic mice (Harbor BioMed, Cambridge, MA) were utilized under a collaboration between the Icahn School of Medicine at Mount Sinai and Harbor BioMed. The H2L2® transgenic mouse is a chimeric transgenic mouse containing a human variable gene segment loci of the heavy and kappa antibody chains along with the rat heavy and kappa constant gene segment loci, producing a mouse with normal B cell homeostasis and effector functions; while also producing antibodies that represent the typical diversity observed in human antibody immunity.[59] Immunizations were performed on eight-to twelve-week-old H2L2® mice interperitoneally with recombinant SARS-CoV2 Spike $RBD_{319\text{-}591}$-Fc fusion protein generated from sequence from the original Wuhan seafood market pneumonia virus isolate (Genbank: MN908947) and cloned in-frame into pcDNA vectors containing human IgG1 and mouse IgG2a Fc tags (GenScript USA Inc., Piscataway, NJ). Each mouse received a prime (50 μg/animal) followed by 2 boosts (100ug/animal), and blood was collected from the submandibular vein two weeks after each boost to monitor titer of sera antibodies. Following sera binding and neutralization analysis, two mice were selected for hybridoma fusion and received two final boosts consisting of 50 μg of the RBD protein at −5 and −2 days before being euthanized by IACUC approved methods with spleens harvested and a final bleeding collected for sera analysis ("fusion sera"). The spleens were processed to single cell suspension and hybridomas were generated using standard protocols (StemCell Technologies, Vancouver, BC, Canada). Briefly, splenocytes were extracted from spleens to single suspension and mixed in a 5:1 ratio with Sp2/0 myelomic fusion partners in the presence of ClonalCell HY-PEG (StemCell Technologies). Individual B cell clones were grown

on soft agar containing HAT (hypoxanthine, aminopterin, thymidine) selection media and selected for screening using a robotic ClonaCell Easy Pick instrument (Hamilton/Stem Cell Technologies). Individual clones were expanded in hybridoma growth media, and the supernatants were used to screen for binding and neutralization assays. All animal studies were approved by the Icahn School of Medicine Institutional Animal Care and Use Committee (IACUC).

Hybridoma Screening: Expi293F cells were transiently transfected to express SARS-CoV-2 spike (Wuhan) using Lipofectamine 3000 (L3000001, Thermo Fisher) and then incubated with supernatant at different dilutions from the hybridoma cell lines from each fusion. Binding was detected using a goat anti-rat (heavy chain specific) APC detection antibody (Jackson ImmunoResearch) and samples were analyzed on a high-throughput flow cytometer (Intellicyte High Throughput Flow Cytometer [Intellicyte Corp., Albuquerque, NM]. Samples were compared to controls of fusion sera, unimmunized "normal" mouse sera, and an in-house generated anti-SARS1/2 Spike mouse monoclonal 2B3E5 at 1 μg/mL. Cells with a high mean fluorescence intensity (MFI) were identified using FlowJo software (Tree Star, Inc.) and graphed using GraphPad Prism to create a heatmap based on mean fluorescence intensity.

ELISA: Immulon 4 HBX high binding clear flat bottom 96 well plates (ThermoFisher) were coated with SARS-CoV2 Spike $RBD_{319\text{-}591}$-Fc fusion at 5 μg/mL in 1xPBS overnight at 4°C followed by washing. Washing with 1xPBS was done between each step in triplicate using a Biotek ELX405 Multi-Plate Washer (Biotek, Winooski, VT). Plates were blocked for 2 h in blocking solution (1xPBS, 0.5% BSA). Supernatants from the hybridomas were then added and allowed to incubate for 1 h at room temperature followed by the addition of goat anti-rat IgG (heavy chain specific)-HRP (Jackson ImmunoResearch) at a 1:5,000 dilution in blocking solution for 1 h. ABTS substrate solution (ThermoFisher) was added and allowed to incubate for 5–10 min at room temperature, protected from light. Absorbance at 450nm was measured using a Biotek Synergy HT Microplate Reader. Fusion sera, normal mouse sera, and 2B3E5 mAb (0.5–1 μg/mL) were used as controls.

Neutralization: Prior to neutralization, hybridoma supernatants grown in SFM (sera free hybridoma media) (Invitrogen) were quantitated using an Octet Red96 by diluting supernatants 1:5 and 1:10 in sera free media and measured for binding against the Anti-Murine IgG Quantitation (AMQ) Biosensors (with cross reactivity to rat IgG Fc) on an Octet Red 96 BLI Instrument (SartoriusAG, Goettingen, Germany). Results were compared to in-lab derived purified rat IgG standards diluted in SFM in the range of 0.5–50 μg/mL. For neutralization, VsV-SARS-CoV-2-spike GFP-expressing reporter virus ($VsV^{CoV2-spike}$) was pre-incubated with mouse sera (1:100-1,200) and hybridoma supernatants (1:10-1:10,000), followed by incubation at 4°C for 1 h before the inoculum was added to HEK-293 cells expressing human ACE2 and Transmembrane Serine Protease-2 overnight at 37°C, 5% CO_2. The cells were harvested and resuspended in cold FACS buffer and analyzed by flow cytometry (Intellicyte Corp., Albuquerque, NM) for GFP fluorescence intensity. Cells with a high MFI were identified using FlowJo software (Tree Star, Inc.) and graphed using GraphPad Prism to create a heatmap based on MFI.

Sequencing and humanizing of antibodies

Sequence of the human variable heavy and kappa chains were obtained by using SMARTer 5′ RACE technology (Takara Bio USA) adapted for antibodies to amplify the variable genes from heavy and kappa chains for each hybridoma. Briefly, RNA

was extracted from each hybridoma using Qiagen RNeasy Mini Kit (Qiagen, Valencia, CA), followed by first stand cDNA synthesis using constant gene specific 3′ primers (GSP1) built in the CH1 exons of the various rat IgG and kappa isotypes and incubated with the SMARTer II A Oligonucleotide and SMARTscribe reverse transcriptase (Rat_G1_G2b_GSP1: 5′-GGCTCAGGGAAATAGCCCTTGA-3′; Rat_G2c_GSP1: 5′-GGCTCAGGGAAATAGCCTTTGA-3′; Rat_cK_GSP1: 5′-GTAACACTGTCCAGGA CACCATC-3′) Amplifying PCR of the first stand cDNA product was then performed using SeqAmp DNA Polymerase (Takara) with a nested 3′ primer (GSP2) specific to the constant genes and a 5′ universal primer based on universal primer sites added to the 5′ end during cDNA generation (Rat_G1_GSP2: 5′ACTTTTGAGAGCAG TTCCAGGAGC-3′; Rat_G2b_GSP2: 5′-GGTTGTATCACCACATCCAGGAGC-3′; Rat_G2c_GSP2: 5′-AGATGTGCCACTGCATCCAGGGAC-3′; Rat_cK_GSP2: 5′-CAG TTGCTAACTGTTCCGTGGATG-3′). Purified PCR product was then submitted for Sanger sequencing using 3′ constant GSP2 primers (GeneWiz, South Plainfield, NJ). Sequence results were blasted against the IMGT human databank of germline genes using V-Quest (http://imgt.org) and analyzed for clonality based on CDR3/ junction identity and V(D)J usage. Unique clones were chosen from each clonal family, and DNA was synthesized and cloned in-framed into pcDNA-based vectors containing a human IgG1 constant region and a human kappa light chain constant region (GenScript USA Inc., Piscataway, NJ).

Formulation of STI-9199

Intranasal formulation was prepared in the form of solution that contains the active pharmaceutical ingredient (nAb) and excipients including buffering agents, stabilizers and a mucoadhesive agent. pH value of the formulation is approximately 5.8 to make suitable for intranasal administration.

Synthesis of comparison antibodies

Antibody expression vector construction and antibody transient expression and purification were done following standard protocols. Briefly, heavy chain and light chain variable domain genes were designed by coding the amino acid sequences of an antibody using codon table of *Cricetulus griseus* for CHO (Chinese hamster ovarian) cells as expression host. The heavy chain and light chain variable domain gene fragments with flanking sequences for infusion cloning were synthesized by IDT (Integrated DNA technologies, San Diego), and cloned into a mammalian expression vector with built-in IgG1 constant domain and/or light chain constant domain sequences. The expression vectors were confirmed by DNA sequencing. CHO-S cells in exponential phase at a cell density of 10^6 cells/mL with viability of $\geq$93%, were co-transfected with both heavy and light chain expression plasmids of the target antibody. The transfection complex was formed between DNA and PEI (polyethylenimine). Each antibody was harvested by centrifuging the culture to pellet and remove the cells 10–14 days after the transfection. The supernatant was processed with a protein A column, and the Protein A bound antibody was eluded with low pH glycine buffer. Purity of the antibodies were analyzed by SDSPAGE to be more than 95%.

The HC constant domain sequence used for all reference clone antibodies is the Mongolian version. Reference clone sequences can be found in supplemental information.

Reference for antibody clone sequences is as follows; S309 (https://www.kegg.jp/entry/D12014); COV2-2130 and COV2-2196 (https://www.genome.jp/entry/D11993) (https://www.genome.jp/entry/D11994); LY-CoV1404 (https://www.rcsb.org/structure/7MMO).

Antibody characterization

Kinetic interactions between the antibodies and His-tagged antigen proteins were measured at room temperature using Biacore T200 surface plasmon resonance (GE Healthcare). Anti-human fragment crystallizable region (Fc region) antibody was immobilized on a CM5 sensor chip to approximately 8,000 resonance units (RU) using standard N-hydroxysuccinimide/N-Ethyl-N′-(3-dimethylaminopropyl) carbodiimide hydrochloride (NHS/EDC) coupling methodology. The antibody (1.5 μg/mL) was captured for 60 s at a flow rate of 10 μL/min. The SARS-CoV-2 Spike S1, SARS-CoV-2 (2019-nCoV) Spike S1- B.1.1.7 lineage mut (HV69-70 deletion, Y144 deletion, N501Y, A570D, D614G, P681H)-His and SARS-CoV-2 (2019-nCoV) Spike S1- B.1.351 lineage mut (K417N, E484K, N501Y, D614G)-His proteins were run at six different dilutions in a running buffer of 0.01 M HEPES pH 7.4, 0.15 M NaCl, 3 mM EDTA, 0.05% v/v Surfactant P20 (HBS-EP+). All measurements were conducted in HBS-EP + buffer with a flow rate of 30 μL/min. The affinity of antibody was analyzed with BIAcore T200 Evaluation software 3.1. A 1:1 (Langmuir) binding model is used to fit the data.

Cell-based SARS-CoV-2 spike-binding assay

Mammalian expression vectors were constructed by cloning the synthesized gene fragments encoding SARS-CoV-2 Spike variant proteins (see Table S1 indicating mutations introduced into wild type [WA-1 strain] spike protein sequence). HEK293 cells were transfected using FuGeneHD transfection reagent according to manufacturer's protocol (Promega, Cat #E2311). 48 h post-transfection, cells were harvested using enzyme free cell dissociation buffer (ThermoFisher, Cat #13151014), washed once and resuspended in FACS buffer (DPBS +2% FBS) at 2×10^6 cells/mL. For antibody binding to the cells expressing the Spike proteins, the cells were dispensed into wells of a 96-well V bottom plate (40 μL per well), and an equal volume of 2x final concentration of serially-diluted anti-S1 antibody solution was added. After incubation on ice for 45 min, the cells were washed with 2 times of 150 μL FACS buffer. Detection of bound antibody was carried out by staining the cells with 50 μL of 1:500 diluted APC AffiniPure F(ab')$_2$ Fragment (Goat Anti-Human IgG (H + L). Jackson ImmunoResearch, Cat# 109-136-4098) for 20 min on ice. The cells were washed once with 150 μL FACS buffer and analyzed on IntelliCyt iQue Screener (Sartorius) flow cytometry. Mean fluorescent intensity values were obtained from the histograms. A sigmoidal four-parameter logistic equation was used for fitting the MFI vs. mAb concentration dataset to extract EC50 values (GraphPad Prism 8.3.0 software).

Cells and viruses

Vero E6 cells were maintained in Dulbecco's modified Eagle's medium (DMEM, Corning, NY) supplemented with 10% fetal bovine serum (FBS, Thermo Fisher Scientific, MA), 1% penicillin–streptomycin, and L-glutamine. The P3 stock of the SARS-CoV-2 USA/WA-1/2020, 202,001, USA/CA-CDC5574/2020 and, MD-HP01542/2021 isolates were obtained from The World Reference Center for Emerging Viruses and Arboviruses (WRCEVA) at the University of Texas Medical Branch. The viruses were propagated in Vero E6 cells and cell culture supernatant of P4 stocks were stored at −80°C under BSL3 conditions.

Baby hamster kidney 21 (BHK21) cells (ATCC #CCL-10) were maintained in DMEM/F12 media (Thermo Fisher #21041025) supplemented with 10% fetal bovine serum (Omega Scientific #FB-02) and 5% tryptose phosphate broth (Thermo Fisher #18050039). BHK21/WI-2 cells (Kerafast #EH1011) were maintained in DMEM (Thermo Fisher #11965092) supplemented with 5% fetal bovine serum. 293-ACE2

cells were maintained in DMEM supplemented with 10% fetal bovine serum and 200 μg/mL G418 (Invivogen #ant-gn-2). HEK-Blue 293 hACE2-TMPRSS2 cells (Invivogen #hkb-hace2tpsa) were maintained in DMEM supplemented with 10% fetal bovine serum, 0.5 μg/mL puromycin (Invivogen #ant-pr-1), 200 μg/mL hygromycin-B (Invivogen #ant-hg-1), and 100 μg/mL zeocin (Invivogen #ant-zn-1).

SARS-CoV-2 viruses were obtained from BEI Resources (Washington strain NR-52281; Alpha variant NR-54000; Beta Variant NR-54009; Gamma variant NR-54982; Delta variant NR- 55611 or NR-55672; Lambda variant NR- 55654: Omicron Variant NR-65461) VeroE6 monolayers were infected at a multiplicity of infection (MOI) of 0.01 in 5 mL virus infection media (DMEM +2% FCS +1X Pen/Strep). Tissue culture flasks were incubated at 36°C and slowly shaken every 15 min for a 90-min period. Cell growth media (35 mL) was added to each flask and infected cultures were incubated at 36°C/5% CO2 for 48 h. Media was then harvested and clarified to remove large cellular debris by room temperature centrifugation at 5,000Xg.

SARS-CoV-2 neutralization assay (ISMMS)

Vero E6 cells stably expressing human ACE2 and TMPRSS2 plated (5,000 cells/well) in a μClear, Black 96-well tissue culture plate (Greiner Bio-One, USA) were in infected with SARS-CoV-2 Washington, Delta (B.1.617.s), or Omicron (B.1.1.529) strains at MOI 0.1 (500 pfu, titered on Vero E6-hACE2-hTMPRSS2) that were pre-incubated (40 min at room temperature) with decreasing concentrations (5–0 mg/mL in 5-fold dilutions) of isotype human IgG1 antibody or anti-SARS-CoV-2 antibody STI-9167. Following a 40 min of infection, the virus/antibody mixture was removed, media added, and cells were incubated for 24 h in 37°C incubator with 5% CO2. Then, cells were fixed with 4% formaldehyde in 1xPBS, permeabilized with 0.1% Triton X-100 in 1xPBS, blocked with 3% BSA in 1xPBS and were stained for nucleus ((4′,6-diamidino-2-phenylindole (DAPI) reagent, 1 μg/mL) and SARS-CoV2 NP (mouse monoclonal anti-SARS2-CoV2 NP 1c7c7 (1 μg/mL) or anti-SARS-CoV-2 spike S2 monoclonal antibody (Sinobiological, #40590-D001) followed by an Alexa Fluor 488-conjugated goat anti-mouse secondary antibody (1 μg/mL). The cells were imaged using a Celigo cytometer (Nexelcom Bioscience) to quantify nuclear and NP stainings. The percent infection was calculated by number of infected cells, i.e. NP + cells, among all cells (DAPI + cells), for each well and normalized to the percent infection of no antibody controlled and plotted as percentages using GraphPad Prism. The IC_{50} values were determined using the [Inhibitor] vs. response - Variable slope (four parameters) analysis.

SARS-CoV-2 neutralization assay

The day before infection, 2×10^4 Vero E6 cells were plated to 96-well plates and incubated at 37 °C, 5% CO_2. Monoclonal antibodies were 2-fold serially diluted in infection media (DMEM+2% FBS). Sixty microliters of diluted samples were incubated with 200 μL of 50% tissue culture infective doses ($TCID_{50}$) of SARS-CoV-2 in 60 μL for 1 h at 37°C. One-hundred microliters of the antibody/virus mixture were subsequently used to infect monolayers of Vero E6 cells grown on 96-well plates. Cells were fixed with 10% formalin and stained with 0.25% crystal violet to visualize cytopathic effect (CPE). The neutralizing concentrations of monoclonal antibodies were determined by complete prevention of CPE.

Plasmids

All SARS-CoV-2 Spike constructs for pseudotype generation were expressed from plasmid pCDNA3.1 (ThermoFisher #V79020). Codon optimized SARS-CoV-2 Wuhan-1 spike carrying the D614G amino acid change (Sino Biological

#VG40589-UT (D614G)) was modified to remove the last 21 amino acids at the C-terminus (SpikeΔ21) and was used as the parental clone. Amino acid changes for each variant are as follows. Alpha: Δ69-70, Δ144, N501Y, A570D, D614G, P681H, T716I, S982A, and D1118H. Beta: D80A, D215G, Δ242–244, K417N, E484K, N501Y, D614G, and A701V. Epsilon: S13I, W152C, L452R, and D614G. Kappa: G142D, E154K, L452R, E484Q, D614G, P681R, Q1071H, and H1101D. Delta: T19R, G142D, Δ156–157, R158G, L452R, T478K, D614G, P681R, and D950N. Delta Plus: T19R, G142D, Δ156–157, R158G, K417N, L452R, T478K, D614G, P681R, and D950N. Gamma: L18F, T20N, P26S, D138Y, R190S, K417T, E484K, N501Y, D614G, H655Y, and T1027I. Zeta: E484Q, F565L, D614G, and V1176F. Lambda: G75V, T76I, R246N, Δ247–253, L452Q, F490S, D614G, and T859N. B.1.1.318: T95I, ΔY144, E484K, D614G, P681H, and D796H. Mu: T95I, Y144T, Y145S, ins146N, R346K, E484K, N501Y, D614G, P681H, and D950N. Omicron: A67V, del69–70, T95I, G142D, del143–145, N211D, del212, G339D, S371L, S373P, S375F, K417N, N440K, G446S, S477N, T478K, E484A, Q493R, G496S, Q498R, N501Y, Y505H, T457K, D614G, H665Y, N679K, P681H, N764K, D796Y, N856K, Q954H, N969K, L981F. Plasmids carrying Spike with single amino acid changes were all generated in Wuhan Spike with a D614G change.

VSV-spike pseudotype generation

To generate each spike pseudotyped VSV, 1.2×10^6 BHK21 cells were nucleofected with 2 μg of spike plasmid using an Amaxa Nucleofector II with cell line kit L (Lonza #VCA-1005) and program A-031. Cells were plated to one well of a 6-well dish and incubated overnight at 37°C/5%CO_2. The next day, cells were transduced with G-Pseudotyped ΔG-luciferase (G*ΔG-luciferase) rVSV (Kerafast #EH1025-PM) at MOI~4 for 1 h at 37°C/5%CO_2. Cells were rinsed twice with DPBS (Corning #21-031-CM), 2 mL of fresh media added, and incubated for 24–44 h at 37°C/5%CO_2. Supernatants were collected, spun at 300*g* for 5 min at room temperature, aliquoted and stored at −80°C. Pseudotyped virus transduction was normalized for luciferase expression by incubating with 1 μg/mL anti-VSV-G clone 8G5F11 (Millipore #MABF2337) for 30 min at room temperature followed by transduction of 293-ACE2 cells. G*ΔG-luciferase VSV of known titer was used as the standard. Transduced cells were incubated for 24 h, 40 μL of ONE-Glo reagent (Promega #E6110) added and luminescence measured using a Tecan Spark plate reader.

Pseudotyped virus particle neutralization assays

HEK-Blue 293 hACE2-TMPRSS2 cells were plated to white-walled 96-well plates at 40K cells/well and incubated at 37°C/5% CO_2. The next day, pseudotyped VSV particle was incubated with anti-spike (concentration as indicated) and anti-VSV-G (1 μg/mL) antibodies for 30 min at room temperature and added to the HEK-Blue 293 hACE2-TMPRSS2 cells in triplicate. Transduced cells were incubated for 24 h, 40 μL of ONE-Glo reagent (Promega #E6110) added and luminescence measured using a Tecan Spark plate reader. The percent inhibition was calculated using 1-([luminescence of antibody treated sample]/[average luminescence of untreated samples]) x 100. Absolute IC_{50} was calculated using non-linear regression with constraints of 100 (top) and 0 (baseline) using GraphPad Prism software. The average of triplicate samples in each of at least 3 independent experiments were included in the analyses for all full variants. For Spike carrying single amino acid changes the average of triplicate samples in each of 2 independent experiments were included in the analyses. Negative value slopes were assigned IC50 of >10 μg/mL. IC_{80} values were calculated using non-linear regression with F = 80 and constraints of 100 (top) and 0 (bottom). For antibody comparison experiments, data for Omicron and Omicron + R346K is an average of 2 independent experiments.

Affinity measurements

Kinetic interactions between the antibodies and His-tagged antigen proteins were measured at room temperature using Biacore T200 surface plasmon resonance (GE Healthcare). Anti-human fragment crystallizable region (Fc region) antibody was immobilized on a CM5 sensor chip to approximately 8,000 resonance units (RU) using standard N-hydroxysuccinimide/N-Ethyl-N′-(3-dimethylaminopropyl) carbodiimide hydrochloride (NHS/EDC) coupling methodology. The antibody (0.5–1 μg/mL) was captured for 60 s at a flow rate of 10 μL/min. Each of the following five variants of SARS-CoV-2 Spike S1 proteins were run at six different dilutions in a running buffer of 0.01 M HEPES pH 7.4, 0.15 M NaCl, 3 mM EDTA, 0.05% v/v Surfactant P20 (HBS-EP+). All measurements were conducted in HBS-EP + buffer with a flow rate of 30 μL/min. The affinity of antibody was analyzed with BIAcore T200 Evaluation software 3.1. A 1:1 (Langmuir) binding model is used to fit the data.

1. Spike S1 (wt)
2. Spike S1 (UK): HV69-70 deletion, Y144 deletion, N501Y, A570D, D614G, P681H)
3. Spike S1 (SA): K417N, E484K, N501Y, D614G
4. Spike S1 (BZ): L18F, T20N, P26S, D138Y, R190S, K417T, E484K, N501Y, D614G, H655Y
5. Spike S1 (DT): T19R, G142D, E156G, 157-158 deletion, L452R, T478K, D614G, P681R
6. Spike S1 (Omicron): A67V, del69-70, T95I, G142D, del143-145, N211D, del212, G339D, S371L, S373P, S375F, K417N, N440K, G446S, S477N, T478K, E484A, Q493R, G496S, Q498R, N501Y, Y505H, T457K, D614G, H665Y, N679K, P681H, N764K, D796Y, N856K, Q954H, N969K, L981F

Biodistribution study

Female CD-1-IGS mice (strain code #022) were obtained from Charles River at 6–8 weeks of age with a weight range of 22–28.8 g. For intravenous injection of 10A3YQYK, 100 μL of antibody diluted in 1X formulation buffer C was administered retro-orbitally to anesthetized animals as previously described.[14] For intranasal injections, antibody was diluted in 1X formulation buffer C and administered by inhalation into the nose of anesthetized animals in a total volume of 20–25 μL using a pipette tip. Organs, blood, and lung lavage samples were collected 24 h post-antibody administration. Blood was collected by retro-orbital bleeding and then transferred to Microvette 200 Z-Gel tubes (Cat no# 20.1291, lot# 8071211, SARSTEDT). Tubes were then centrifuged at 10,000*g* for 5 min at room temperature. Serum was transferred into 1.5 mL tubes and stored at −80°C. Lung lavage samples were collected following insertion of a 20G x 1-inch catheter (Angiocath Autoguard, Ref# 381702, lot# 6063946, Becton Dickinson) into the trachea. A volume of 0.8 mL of PBS was drawn into a syringe, placed into the open end of the catheter, and slowly injected and aspirated 4 times. The syringe was removed from the catheter, and the recovered lavage fluid was transferred into 1.5 mL tubes and kept on ice. Lavage samples were centrifuged at 800*g* for 10 min at 4°C. Supernatants were collected, transferred to fresh 1.5 mL tubes, and stored at −80°C. Total spleen, total large intestine, total lungs and 200 to 250 mg of small intestine were suspended in 300 μL of PBS in pre-filled 2.0 mL tubes containing zirconium beads (cat 155-40945, Spectrum). Tubes were processed in a BeadBug-6 homogenizer at a speed setting of 3,000 and a 30 s cycle time for four cycles with a 30-s break after each cycle. Tissue homogenates were centrifuged at 15,000 rpm for 20 min at 4°C. Homogenate supernatants were then transferred into 1.5 mL tubes and stored at −80°C. STI-9167 antibody levels in each sample were quantified using the antibody detection ELISA

method. Statistical significance was determined using the Welch's t-test. This study was reviewed and accepted by the animal study review committee (SRC) and conducted in accordance with IACUC guidelines.

Pharmacokinetic study

Female CD-1-IGS (strain code #022) were obtained from Charles River Laboratories at 6–8 weeks of age with a weight range of 20.3–26.3 g. STI-9167 was dissolved in intranasal formulation buffer C was administered as previously described for the IN biodistribution study. Lungs and blood were collected from 6 mice at each of the following timepoints: 10 min, 1.5 h, 6 h, 24 h, 72 h, 96 h, 168 h, 240 h, and 336 h. Serum and lung tissue samples were collected as described for the biodistribution study. STI-9167 antibody levels in each sample were quantified using the antibody detection ELISA method. Pharmacokinetic analysis of the collected ELISA data was performed with the Phoenix WiNnonlin suite of software (version 6.4, Certara) using a non-compartmental approach consistent with an IN-bolus route of administration. Statistical significance was determined using the Welch's t-test. This study was reviewed and accepted by the animal study review committee (SRC) and conducted in accordance with IACUC guidelines.

khACE2 mouse model of COVID-19 infection

Female K18-hACE2 transgenic mice were purchased from Jackson laboratory and maintained in pathogen-free conditions and handling conforms to the requirements of the National Institutes of Health and the Scripps Research Institute Animal Research Committee. 8–12 weeks old mice (weight range of 16.2–29.1 g) were infected intranasally with 10,000 PFU of SARS-COV-2 in total volume 50 μL different concentration of AB were injected intravenously 1 h post infection or by intranasal instillation 12 h post infection using Palivizumab as the Isotype control, STI-9167 or STI-9199 depending on the route of administration.

Determination of infectious virus titer in the lung

On day 4 post-infection, animals were euthanized, lung tissue samples were collected from each animal, and the left lobe of each collected lung was placed into a pre-labeled microcentrifuge tube containing 3–5 beads 2.3 mm diameter Zirconia/silica beads (Fischer). Lung samples were homogenized with DMEM +5% FBS in a TissueLyser 1 min 25 s.[60]

VeroE6 cells were plated at 3.0E+05 cells/well in 24 well plates in volume 400 μL/well. After 24 h medium was removed, and serial dilution of homogenized lungs were added to Vero cells and subsequently incubated for 1 h at 37°C. After incubation, an overlay (1:1 of 2% methylcellulose [Sigma] and culture media) is added to each well and incubation commenced for 3 days at 37°C. Plaque staining was performed using Crystal Violet as mentioned above. Virus titers in lungs were compared with the isotype control mAb-treated group using a Student's *t* test.

Plaque reduction neutralizing assay

VeroE6 cells were plated at 18.0E+03 cells/well in a flat bottom 96-well plate in a volume of 200 μL/well. After 24 h, a serial dilution of ABs is prepared in a 100 μL/well at twice the final concentration desired and live virus was added at 1,000 PFU/100 μL of SARS-COV-2 and subsequently incubated for 1 h at 37°C in a total volume of 200 μL/well. Cell culture media was removed from cells and sera/virus premix was added to VeroE6 cells at 100 μL/well and incubated for 1 h at 37°C. After incubation, 100 μL of "overlay" (1:1 of 2% methylcellulose (Sigma) and culture media) is added to each well and incubation commenced for 3 d at 37°C. Plaque staining using Crystal Violet (Sigma) was performed

upon 30 min of fixing the cells with 4% paraformaldehyde (Sigma) diluted in PBS. Plaques were assessed using a light microscope (Keyence).

HISTOCHEMICAL STAINING AND ANALYSIS

K18-hACE2 mice were maintained and infected following above methods. On Day 4, mice were euthanized and lung samples were collected, fixed in 1X Alcoholic Z-Fix (Anatech Ltd) for 48 h at room temperature. Samples were then fully processed by HistoWiz, Inc. (Brooklyn, NY), following HistoWiz protocols for H&E staining and IHC.

QUANTIFICATION AND STATISTICAL ANALYSIS

GraphPad Prism 8.3.0 software was primarily used for data analysis and statistics. Methods of quantification and subsequent statistical analysis is described in the relevant methods detail subsections and the corresponding figure legends. Statistical methods were selected based on previous hamster model studies.

Med, Volume *3*

Supplemental information

Discovery and intranasal administration of a SARS-CoV-2 broadly acting neutralizing antibody with activity against multiple Omicron subvariants

J. Andrew Duty, Thomas Kraus, Heyue Zhou, Yanliang Zhang, Namir Shaabani, Soner Yildiz, Na Du, Alok Singh, Lisa Miorin, Donghui Li, Karen Stegman, Sabrina Ophir, Xia Cao, Kristina Atanasoff, Reyna Lim, Ignacio Mena, Nicole M. Bouvier, Shreyas Kowdle, Juan Manuel Carreño, Laura Rivero-Nava, Ariel Raskin, Elena Moreno, Sachi Johnson, Raveen Rathnasinghe, Chin I. Pai, Thomas Kehrer, Elizabeth Paz Cabral, Sonia Jangra, Laura Healy, Gagandeep Singh, Prajakta Warang, Viviana Simon, Emilia Mia Sordillo, Harm van Bakel, Yonghong Liu, Weina Sun, Lisa Kerwin, John Teijaro, Michael Schotsaert, Florian Krammer, Damien Bresson, Adolfo García-Sastre, Yanwen Fu, Benhur Lee, Colin Powers, Thomas Moran, Henry Ji, Domenico Tortorella, and Robert Allen

Supplemental Figure 1.

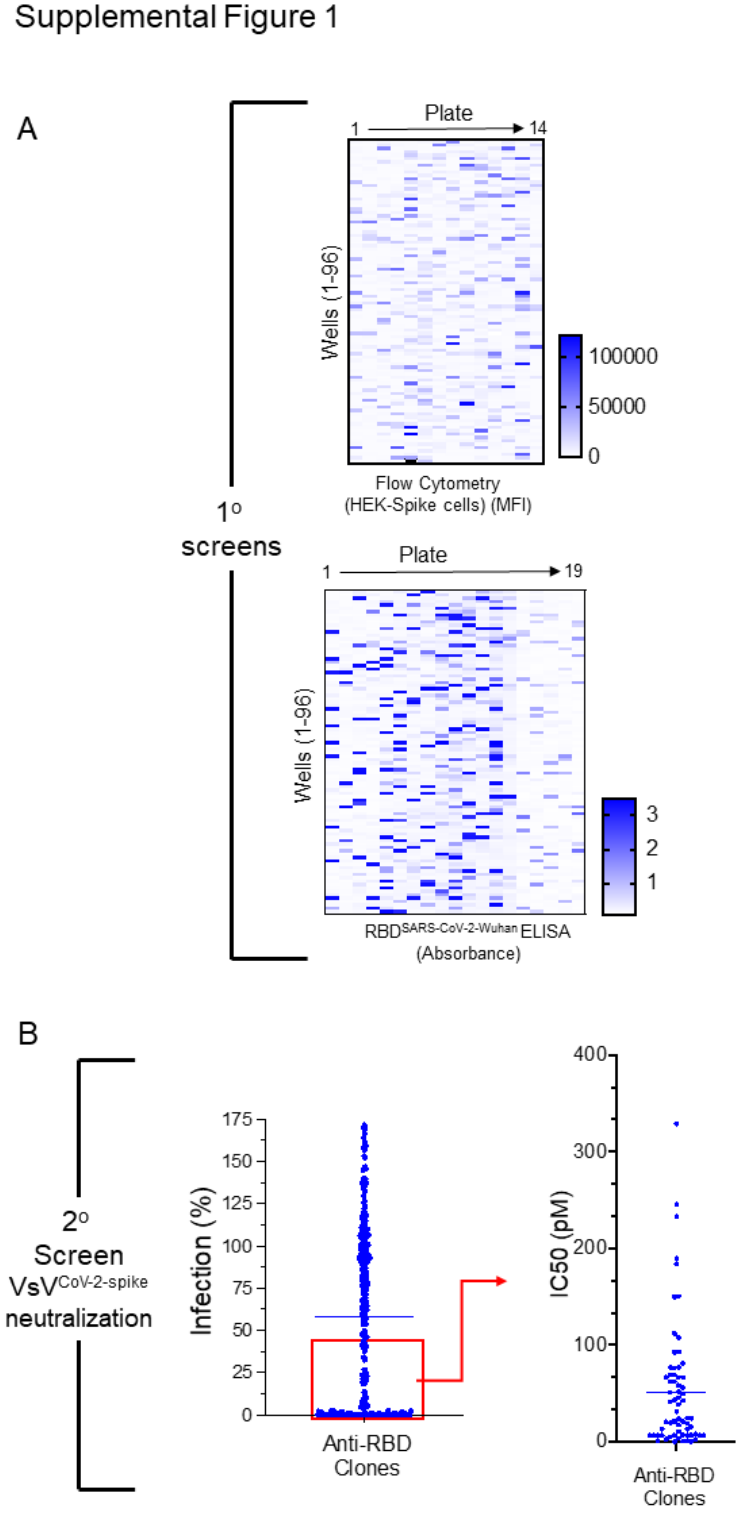

Supplemental Figure 1: Discovery of SARS-CoV-2 Neutralizing Antibodies from Mouse 3. Related to Figure 1.

(A) Primary screens based on the anti-RBD hybridoma clones from mouse 3(M-3) were performed by flow-cytometry using Expi293F cells transfected with SARS-CoV-2 Wuhan strain spike protein and RBD ELISA. Upon flow cytometry analysis, the mean fluorescence intensity (MFI) was determined for each clone. The RBD-ELISA represents binding of the clones to RBD as measured by absorbance. Both the flow cytometry and ELISA data are represented as heat maps. (B) The secondary assays for the binding clones were a VSV-spike^{CoV-2} neutralization assay followed by the determination of IC50 (pM) for clones with > 50% neutralization activity.

Supplemental Figure 2.

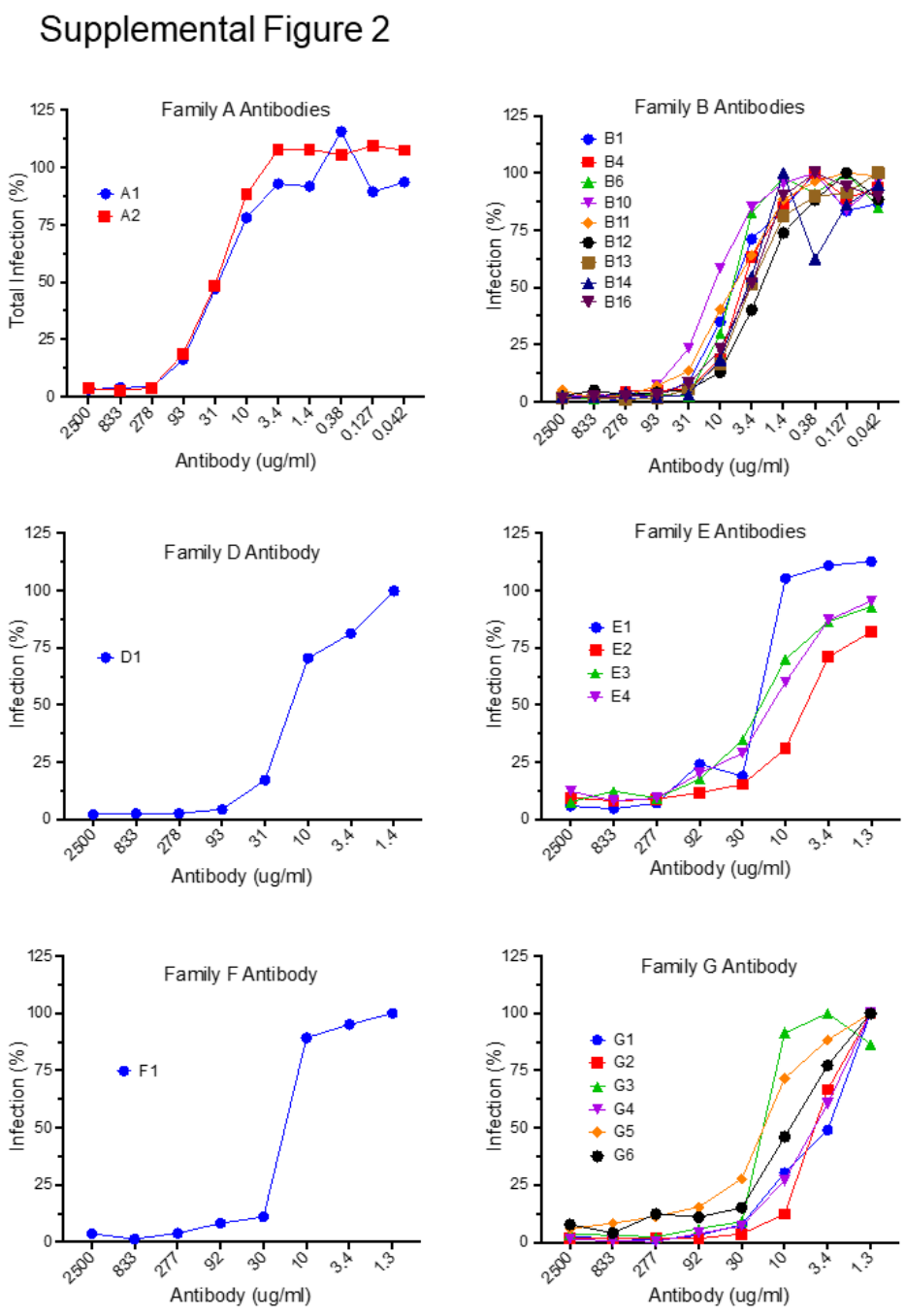

Supplemental Figure 2: Analysis of neutralization activity of anti-SARS-CoV-2 clones.

Related to Figure 1.

HEK-293 expressing hACE2/TMPRSS2 cells (10,000 cells/well of 96 well plate) were infected with VSV-spike^{CoV-2} pre-incubated with increasing concentrations of individual antibodies from the different antibody Families. At 24 hours post-infection, the cells were detached using non-enzymatic dissociation reagent and resuspended in cold FACS buffer and analyzed by flow cytometry (Intellicyte Corp., Albuquerque, NM) for GFP fluorescence intensity. The % of GFP positive cells was identified from each sample and % of GFP positive cells from mock-treated virus was used as 100% infection. The data was normalized to 100% infection and the IC50 was determined by GraphPad Prism using [Inhibitor] vs. normalized response-variable slope.

Supplemental Figure 3.

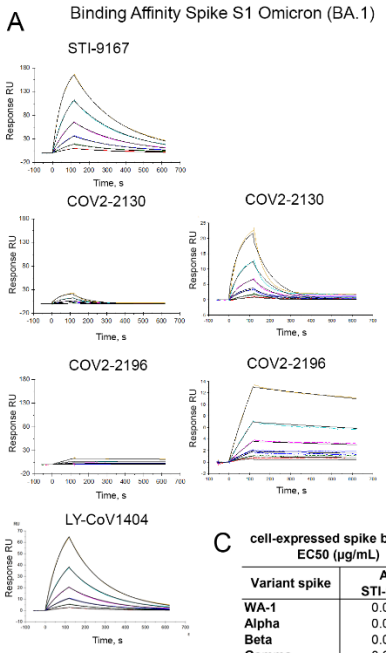

C

cell-expressed spike binding EC50 (μg/mL)

Variant spike	Ab STI-9167
WA-1	0.025
Alpha	0.019
Beta	0.015
Gamma	0.014
Delta Plus	0.043
Lambda	0.0089

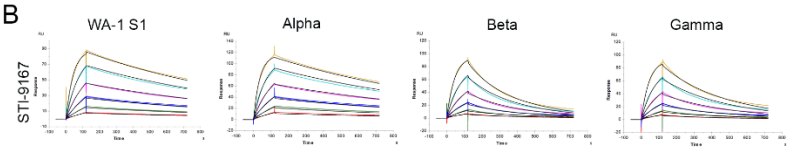

Variant RBD	ka (1/Ms) Ab STI-9167	kd (1/s) Ab STI-9167	KD (M) Ab STI-9167	Rmax (RU) Ab STI-9167	Chi² (RU²) Ab STI-9167
WA-1	2.27 ± 0.2 E+05	1.40 ± 0.03 E-03	6.20 ± 0.44 E-09	97.2 ± 4.3	1.19 ± 0.30
Alpha	2.65 ± 0.2 E+05	1.32 ± 0.03 E-03	5.04 ± 0.04 E-09	105.4 ± 6.5	1.56 ± 0.24
Beta	2.12 ± 0.2 E+05	6.84 ± 0.12 E-03	3.24 ± 0.26 E-08	108.3 ± 6.6	0.14 ± 0.02
Gamma	2.57 ± 0.2 E+05	5.23 ± 0.05 E-03	2.04 ± 0.16 E-08	104.9 ± 5.6	0.53 ± 0.04

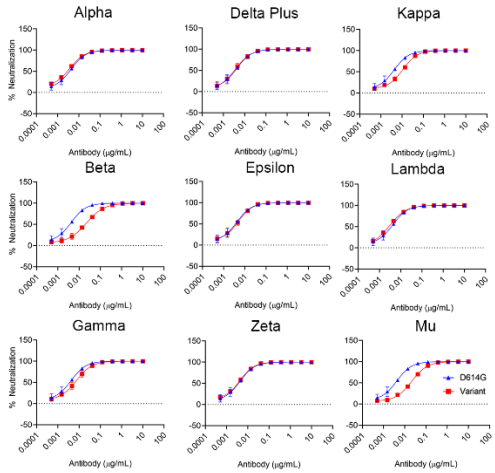

Pseudotype neutralization IC50 (μg/mL)

Virus	Ab STI-9167
Alpha	0.0029
Beta	0.0195
Gamma	0.0063
Delta Plus	0.0033
Epsilon	0.0040
Zeta	0.0034
Kappa	0.0090
Lambda	0.0027
Mu	0.0186

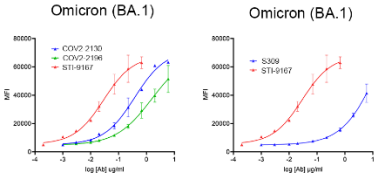

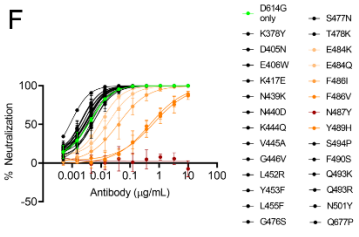

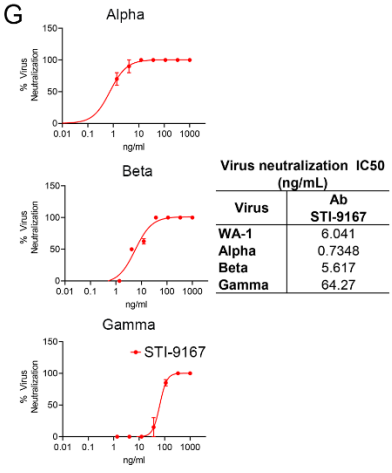

Virus neutralization IC50 (ng/mL)

Virus	Ab STI-9167
WA-1	6.041
Alpha	0.7348
Beta	5.617
Gamma	64.27

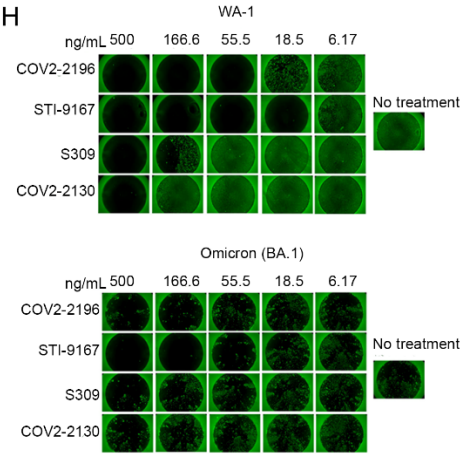

Supplemental Figure 3. Binding and neutralization of candidate antibody to VoCs.

Related to Figure 2. (A) SPR binding affinity graphs of antibodies STI-9167, COV2-2130, COV2-2196, and S309. (B) Affinity measurements of STI-9167 against the Spike S1 binding domain from SARS-CoV-2 isolates and VOCs: USA/WA-1/2020(WA-1) isolate, Alpha, Beta, and Gamma. The antibody affinities were measured using SPR on a BIAcore T200 instrument using a 1:1 binding model. Graphs are representative of triplicate data and table data presented as mean ± SD. (C) Spike protein derived from Alpha, Beta, Gamma, Delta Plus, and Lambda SARS-CoV-2 isolates were independently expressed on the surface of HEK 293 cells. Serially-diluted STI-9167 was assayed for spike protein binding to the transfected spike cells by flow cytometry. To quantify antibody binding, mean fluorescent intensity was measured for each dilution tested and the EC_{50} value was calculated for each nAb. (D) Spike-pseudotyped VSV neutralization. Antibody neutralization curves of the pseudotyped VSVs spike variants (Material and Methods) is representative of three independent experiments, with error bars representing one standard deviation. IC50 values for each pseudotype/antibody combination are indicated . (D) PRNT assay using STI-9167 withSARS-CoV-2 variants were performed (Material and Methods). (E) Omicron spike protein was expressed on HEK 293 cells and binding of selected neutralizing antibodies was measured by MFI using flow cytometry. (F) Pseudotyped VSVs were generated from vectors of SARS-CoV-2 Spike Wuhan strain carrying the D614G substitution with an additional amino acid substitution in the RBD. Pseudotype VSV-spike neutralization assays were performed using STI-9167 (Materials and Methods, duplicate experimental runs in technical triplicate repeats) to determine the potential structural constraints of STI-9167 neutralization. Curves were generated using non-linear regression with constraints of 100 (top) and 0 (baseline). Parental Spike D614G only is color coded in green. Additional substitutions that led to IC50 values >2 fold higher than

D614G are colored, while all other substitutions are in black. (G) PRNT assay using STI-9167 withSARS-CoV-2 variants were performed to determine IC50 values (μg/ml) (Material and Methods). (H) PRNT assay using STI-9167 and various neutralizing antibodies with SARS-CoV-2 WA-1 or Omicron were performed (Material and Methods) on Vero-ACE2-expressing cells.

Supplemental Figure 4.

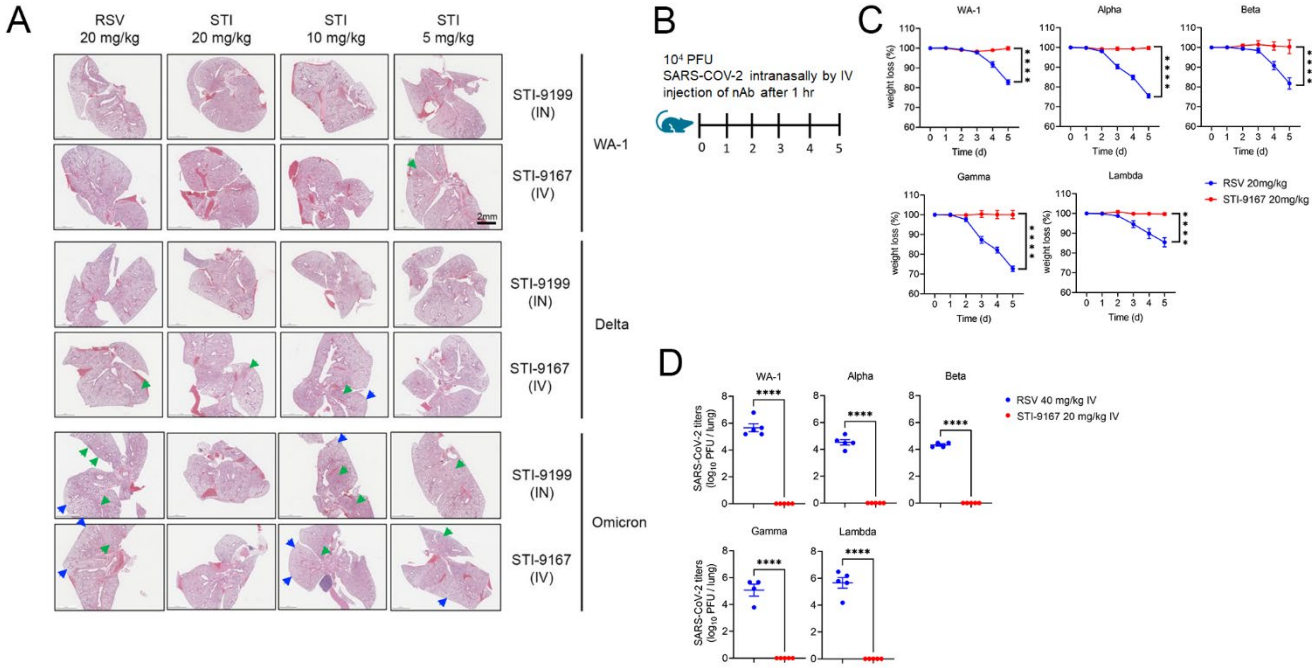

Supplemental Figure 4. Efficacy of Intranasal (IN) delivery of STI-9167 neutralizing antibody in the K18-hACE2 murine model of COVID-19 VOCs.

Related to Figure 4. (A) H&E staining of lung tissue was performed on mice infected with WA-1, Delta and Omicron and treated with indicated concentrations of antibody, either administered IV or IN. Representative images are shown (scale bar, 2 mm). Generally, areas of dense consolidation in H&E sections correspond to virus-infected areas in IHC sections (green arrowheads), while the

aerated/non-consolidated lung parenchyma corresponds to an absence of virus staining in IHC (blue arrowheads). (B) A schematic of experimental model, K18-hACE2 transgenic mice were infected with 10000 PFU of indicated variants of SARS-CoV-2 treated with indicated concentration of nAb (STI-9167) intravenously 1 hour post infection. (C) Body weight change of mice was measured daily (n = 5). (D) SARS-CoV-2 viral titers were measured in lung day 5 post infection (n = 5). P****<0.0001 values were determined using a two-way ANOVA (B) and unpaired t test (D).

Supplemental Table 1. SARS-CoV-2 Variants and Mutations. Related to Methods Section.

Variant	Mutations (and mutations in RBD from 333 to 526)
B1.1.7/Alpha variant	deletion of 69-70, deletion of Y144, N501Y, A570D, D614G, P681H, T716I, S982A, D1118H
B1.351/Beta variant	L18F, D80A, D215G, deletion of 242-244, R246I, K417N, E484K, N501Y, D614G, A701V
P.1/Gamma variant	L18F, T20N, P26S, D138Y, R190S, K417T, E484K, N501Y, H655Y, T1027I
B.1.526/Iota variant	L5F, T95I, D253G, E484K, D614G, A701V
B.1.427/B.1.429/Epsilon variant	S13I, W152C, L452R
B.1.427/B.1.429/Epsilon variant	T478K, D614G
B.1.617.1/Kappa variant	T95I, G142D, E154K, L452R, E484Q, D614G, P681R, Q1071H, H1101D
B.1.617.2/Delta variant	T19R, T95I, G142D, deletion of 157-158, A222V, L452R, T478K, D614G, P681R, D950N
B.1.1.529/Omicron (BA.1) variant	A67V, del69-70, T95I, G142D, del143-145, N211D, del212, G339D, S371L, S373P, S375F, K417N, N440K, G446S, S477N, T478K, E484A, Q493R, G496S, Q498R, N501Y, Y505H, T457K, D614G, H665Y, N679K, P681H, N764K, D796Y, N856K, Q954H, N969K, L981F
B.1.1.529/Omicron + R346K (BA.1.1) variant	A67V, del69-70, T95I, G142D, del143-145, N211D, del212, G339D, R346K, S371L, S373P, S375F, K417N, N440K, G446S, S477N, T478K, E484A, Q493R, G496S, Q498R, N501Y, Y505H, T457K, D614G, H665Y, N679K, P681H, N764K, D796Y, N856K, Q954H, N969K, L981F
BA.2	T19I, L24S, del25-27, G142D, V213G, G339D, S371F, S373P, S375F, T376A, D405N, R408S, K417N, N440K, S477N, T478K, E484A, Q493R, Q498R, N501Y, Y505H, H655Y, N679K, P681H, N764K, D796Y, Q954H, N969K